Article

Broad Spectrum Functional Activity of Structurally Related Monoanionic Au(III) Bis(Dithiolene) Complexes

**Yann Le Gal [1], Agathe Filatre-Furcate [1], Dominique Lorcy [1,*], Olivier Jeannin [1], Thierry Roisnel [1], Vincent Dorcet [1],
Diana Fontinha [2], Denise Francisco [2], Miguel Prudêncio [2], Marta Martins [2], Catarina Soeiro [3,4], Sílvia A. Sousa [3,4],
Jorge H. Leitão [3,4], Tânia S. Morais [5], Inês Bártolo [6], Nuno Taveira [6], Joana F. Guerreiro [7] and Fernanda Marques [7,*]**

[1] Université Rennes, CNRS, ISCR (Institut des Sciences Chimiques de Rennes)—UMR 6226,
F-35000 Rennes, France; yann.le-gal@univ-rennes1.fr (Y.L.G.); agathe.filatre@gmail.com (A.F.-F.);
olivier.jeannin@univ-rennes1.fr (O.J.); thierry.roisnel@univ-rennes1.fr (T.R.);
vincent.dorcet@univ-rennes1.fr (V.D.)

[2] Instituto de Medicina Molecular João Lobo Antunes, Faculdade de Medicina, Universidade de Lisboa,
Avenida Professor Egas Moniz, 1649-028 Lisboa, Portugal; dfontinha@medicina.ulisboa.pt (D.F.);
denisefrancisco@medicina.ulisboa.pt (D.F.); mprudencio@medicina.ulisboa.pt (M.P.);
marta.martins@medicina.ulisboa.pt (M.M.)

[3] iBB-Institute for Bioengineering and Biosciences, Departmento de Bioengenharia, Instituto Superior Técnico,
Universidade de Lisboa, Av. Rovisco Pais, 1049-001 Lisboa, Portugal; catarina.soeiro25@gmail.com (C.S.);
sousasilvia@tecnico.ulisboa.pt (S.A.S.); jorgeleitao@tecnico.ulisboa.pt (J.H.L.)

[4] Associate Laboratory, i4HB—Institute for Health and Bioeconomy at Instituto Superior Técnico,
Universidade de Lisboa, Av. Rovisco Pais, 1049-001 Lisboa, Portugal

[5] Centro de Química Estrutural and Departamento de Química e Bioquímica, Faculdade de Ciências,
Universidade de Lisboa, Campo Grande, 1749-016 Lisboa, Portugal; tsmorais@fc.ul.pt

[6] iMed.ULisboa, Faculdade de Farmácia da Universidade de Lisboa, Avenida das Forças Armadas,
1600-083 Lisboa, Portugal; ibartolo@ff.ulisboa.pt (I.B.); ntaveira@ff.ulisboa.pt (N.T.)

[7] Centro de Ciências e Tecnologias Nucleares e Departamento de Ciências e Tecnologias Nucleares,
Instituto Superior Técnico, Universidade de Lisboa, Estrada Nacional 10 (km 139.7),
2695-066 Bobadela, Portugal; joanaguerreiro@ctn.tecnico.ulisboa.pt

* Correspondence: dominique.lorcy@univ-rennes1.fr.fr (D.L.); fmarujo@ctn.tecnico.ulisboa.pt (F.M.)

Abstract: The biological properties of sixteen structurally related monoanionic gold (III) bis(dithiolene/diselenolene) complexes were evaluated. The complexes differ in the nature of the heteroatom connected to the gold atom (AuS for dithiolene, AuSe for diselenolene), the substituent on the nitrogen atom of the thiazoline ring (Me, Et, Pr, iPr and Bu), the nature of the exocyclic atom or group of atoms (O, S, Se, $C(CN)_2$) and the counter-ion (Ph_4P^+ or Et_4N^+). The anticancer and antimicrobial activities of all the complexes were investigated, while the anti-HIV activity was evaluated only for selected complexes. Most complexes showed relevant anticancer activities against Cisplatin-sensitive and Cisplatin-resistant ovarian cancer cells A2780 and OVCAR8, respectively. After 48 h of incubation, the IC_{50} values ranged from 0.1–8 μM (A2780) and 0.8–29 μM (OVCAR8). The complexes with the Ph_4P^+ ([**P**]) counter-ion are in general more active than their Et_4N^+ ([**N**]) analogues, presenting IC_{50} values in the same order of magnitude or even lower than Auranofin. Studies in the zebrafish embryo model further showed that, despite their marked anticancer effect, the complexes with [**P**] counter-ion exhibited low in vivo toxicity. In general, the exocyclic exchange of sulfur by oxygen or ylidenemalononitrile ($C(CN)_2$) enhanced the compounds toxicity. Most complexes containing the [**P**] counter ion exhibited exceptional antiplasmodial activity against the *Plasmodium berghei* parasite liver stages, with submicromolar IC_{50} values ranging from 400–700 nM. In contrast, antibacterial/fungi activities were highest for most complexes with the [**N**] counter-ion. Auranofin and two selected complexes [**P**][AuSBu(=S)] and [**P**][AuSEt(=S)] did not present anti-HIV activity in TZM-bl cells. Mechanistic studies for selected complexes support the idea that thioredoxin reductase, but not DNA, is a possible target for some of these complexes. The complexes [**P**] [AuSBu(=S)], [**P**] [AuSEt(=S)], [**P**] [AuSEt(=Se)] and [**P**] [AuSeiPr(=S)] displayed a strong quenching of the fluorescence intensity of human serum albumin (HSA), which indicates a strong interaction with this protein. Overall, the results highlight the promising biological

activities of these complexes, warranting their further evaluation as future drug candidates with clinical applicability.

1. Introduction

Most of the drugs currently in clinical use to treat cancer, microbial or viral infections present several disadvantages, such as their low selectivity, acquired drug resistance, toxicity and severe side-effects, evidencing the need for the development of novel and more efficient strategies. Metal-based complexes can mitigate most of these disadvantages. In fact, metal complexes have attracted considerable interest mainly due to their versatile electronic and structural features that can be explored for rational drug design. The metal ion, its oxidation state, coordination numbers and geometries and type and number of ligands are some of the key features that must be considered in the design and synthesis of prospective drugs for medical use. In line with this, numerous compounds of different transition metal ions are currently under development or reaching the clinical settings for medical applications [1–4]. Their unique properties offer novel chemistry and provide great opportunities for the discovery of drugs with new mechanisms of action [1,5,6]. In particular, Cisplatin, the well-known platinum drug with a long history in cancer treatment and the knowledge of its side effects, systemic toxicity, mechanism of action, and tumor resistance, has prompted several efforts to explore novel strategies and formulae to develop new metal complexes that exhibit non-classical modes of action with improved balance of risk–benefits [7–10]. In this context, gold complexes have gained much attention and endured extensive research in the medicinal chemistry domain for the treatment of cancer, inflammatory disorders and infectious diseases [11].

The investigation on the anticancer properties of gold complexes was primarily focused on Auranofin, a gold (I) phosphine derivative that has been investigated as a potential treatment for cancer (e.g., leukemia, ovarian), neurodegenerative disorders, HIV/AIDS, as well as parasitic and bacterial infections [10]. Motivated by the broad spectrum of activity of Auranofin, a diversity of gold(I) complexes bearing phosphine ligands such as triphenylphosphine, diphenylphosphino-alkanes and dithiocarbamates have been synthetized and showed potent antiproliferative activity on a variety of cancer cells [12,13]. On the other hand, gold (III) complexes have been studied as potential anticancer agents due to their square-planar geometry, similar to that of Cisplatin [14,15]. In general, gold (I/III) complexes constitute a diverse family of very promising agents for cancer therapy. Indeed, several gold (I/III) complexes have shown outstanding in vitro antiproliferative activities against several types of cancer cells, in some cases opening new prospects for further advanced preclinical studies. Relevant examples are gold(I/III) complexes with polydentate nitrogen donor ligands, (C^N)-cyclometalated ligands and N-heterocyclic carbenes (NHCs) [16–19]. Although some gold-NHC derivatives undergo ligand rearrangement reactions in the presence of water, some other complexes are stable in aqueous environment and showed anticancer activity superior to Cisplatin, which makes these complexes excellent potential chemotherapeutics [20–25].

The mechanisms underlying the antiproliferative activities of gold(I/III) complexes remain unclear [26,27]. In vitro studies showed that Auranofin can overcome Cisplatin resistance in human ovarian cancer cells, which indicates a mode of action different from the one described for Cisplatin. In fact, Auranofin has been identified as a potent inhibitor of thioredoxin reductase (TrxR), due to the high affinity of gold(I) for the selenocysteine residue of TrxR, thus causing an alteration in the cellular redox balance and a cascade of severe metabolic impairments that result in apoptotic cell death. In some cases, the apoptotic response is mediated by mitochondrial membrane potential depolarization and

enhanced caspase activity [19,26–30]. In several cancer cells, high expression levels of TrxR are related to cell growth and proliferation and poor prognosis in a variety of cancers [31].

Interactions with cysteine- or selenocysteine-containing enzymes other than thioredoxin reductase was also reported, such as phosphatases, cathepsin and topoisomerase I [32,33].

Literature examples evidence a DNA-independent mechanism of action for some gold(I/III) complexes, although others report DNA binding, and more recently the binding to DNA secondary structures such as G-quadruplex (G4) nucleic acids. Metal complexes as small G4-ligands are expected to interact selectively with G4 nucleic acids, acting as a promising strategy for the development of anticancer drugs with selective toxicity towards cancer cells over normal ones [34].

The antimicrobial activity of gold(I/III) complexes has not been investigated as extensively as their anticancer activity. Only recently, due to the threat of multidrug-resistant (MDR) pathogens, the application of these compounds as antimicrobials has gained more attention [35]. Nevertheless, a considerable number of gold(I) and gold(III) complexes, mostly complexes with a +1 oxidation state, have been tested against a broad spectrum of bacteria, fungi and parasites. In general, gold(I) complexes with phosphine showed relevant antibacterial and antifungal activities. Auranofin and gold(I/III) complexes with NHC ligands display antimicrobial potential against many Gram-positive bacteria, including multidrug resistant strains, but poor activity towards Gram-negative species. Gold(I/III) complexes with NHCs ligands were found as efficient inhibitors of bacterial TrxR, indicating that inhibition of this enzyme might be involved in their mechanism of action [36].

The activity of Auranofin against different pathogenic fungi, including multidrug-resistant *Candida albicans*, was also demonstrated [37–40].

So far, only a few gold(I/III) complexes have been evaluated as antimalarial compounds. Auranofin was identified in a high-throughput screening as having activity against the hepatic stage of the rodent *Plasmodium berghei* parasite in vitro. Furthermore, it displayed in vitro activity against the blood stage of the 3D7 and Dd2 strains of *P. falciparum* [41].

Promising candidates for future development have been the gold(I/III) complexes containing thiosemicarbazonato, phosphines and NHCs ligands [22,42–45]. The presence of N-containing heterocycles in the series of mononuclear gold(I) complexes is of great importance to the antiplasmodial activity, which is probably related to lipophilicity, basicity, and structural features of these complexes. However, further studies are needed to extensively explore these complexes as antimalarial drugs. The mechanism of action seemed to involve the inhibition of antioxidant systems that are critical for the parasite's survival. In vitro, these complexes have been shown to directly inhibit the parasite's TrxR [21].

Whereas extensive work has been conducted with gold(I) complexes, the high oxidation state counterparts gold(III) have not been explored as much. In view of bridging the gap and making a contribution to explore other relevant gold(III) complexes, our group recently demonstrate the potential activity of monoanionic gold(III) bis(dithiolene) complexes against ovarian cancer cells, Gram-positive bacteria, *Candida* strains and *P. berghei* [46,47]. The interactions of these gold(III) bis(dithiolene) complexes with DNA, the classical cellular target of Cisplatin, are negligible, as was observed for Auranofin, suggesting a different mechanism of action for the observed biological effects [46]. In addition, the results obtained indicate that TrxR could constitute a potential target of gold(III) bis(dithiolene) complexes [47]. These promising results prompted us to herein explore the multifunctional therapeutic potential of a novel series of structurally related mononuclear gold(III) bis(dithiolene) complexes as prospective anticancer, antibacterial, antiplasmodial and anti-HIV drugs. Complexes differing from the ones previously described in [47] by the substituent on the nitrogen atom of the thiazoline ring, the nature of the chalcogen atoms within the metallacycles, sulfur vs. selenium, together with the

exocyclic sulfur replacement and the counter-ion, Ph_4P^+ or Et_4N^+ (Chart 1). The effect of modifications of the ligand skeleton and counter-ion on the biological properties of theses complexes will be discussed.

One of the crucial steps in the development of novel drugs is studying the interaction to albumin, the main blood protein. Surprisingly, studies on the interaction of gold(III) complexes with serum proteins have been poorly explored, despite of their extreme relevance for the mechanism of action, toxic effects, as well as their transport and distribution in vivo [15,48,49]. In the present study, we investigated the interaction of selected complexes with human serum albumin (HSA) by fluorescence spectroscopy, taking advantage of the intrinsic fluorescence of this protein.
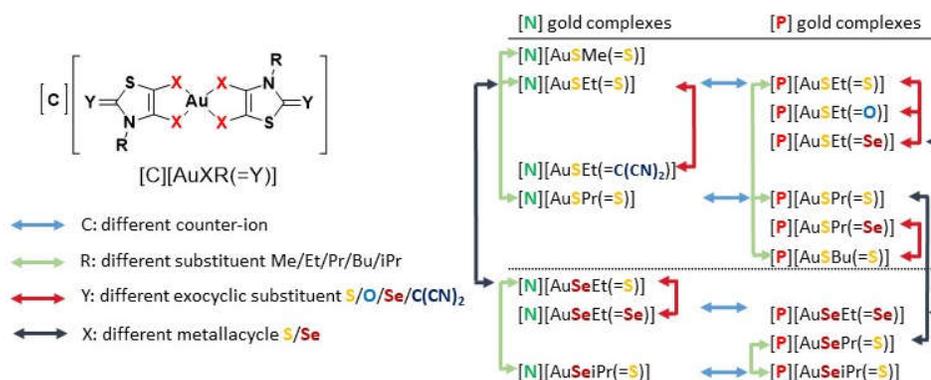

Chart 1. Schematic notation of the Au(III) complexes, [C][AuXR(=Y)], (C = **P** for Ph_4P^+ or **N** for Et_4N^+, X = S or Se, Y = O, S, Se, $C(CN)_2$ and R = Me, Et, Pr, *i*Pr and Bu) and the structure relationships of the series of gold bis(dithiolene/diselenolene) complexes investigated in this study.

2. Results and Discussion

### 2.1. Synthesis and Redox Properties of the Gold Complexes

The general synthetic strategy used to prepare the different gold monoanionic complexes starting from the N-alkyl-1,3-thiazoline-2-chalcogenone **1-R(=Y)** is outlined in Scheme 1. The first step corresponds to the metalation of the heterocyclic ring with lithium diisopropylamide (LDA) followed by the addition of sulfur or selenium and bromopropionitrile, in order to form the protected dithiolene or diselenolene ligand, **2-XR(=Y)** [50]. Then, the deprotection of the dithiolene (X = S) or diselenolene (X = Se) ligand was performed in the presence of sodium methoxide, NaOMe, followed by the subsequent addition of $KAuCl_4 \cdot H_2O$ and Ph_4PCl or Et_4NBr to afford the monoanionic gold complexes, [C][AuXR(=Y)]. After recrystallization in acetonitrile, the gold complexes were isolated as dark greenish crystalline solids. The newly synthesized complexes were all characterized using ^1H NMR, HRMS, elemental analysis and cyclic voltammetry. The sixteen gold complexes prepared and investigated in this study are collected in Chart 1.
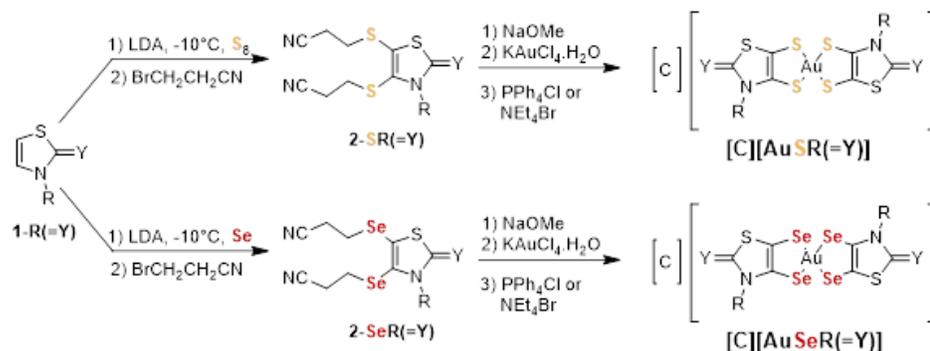
Scheme 1. Synthetic path to the monoanionic gold bis(dithiolene) **[C][AuSR(=Y)]**, (C = Ph$_4$P$^+$, Et$_4$N$^+$, R = Me, Et, Pr, Bu and Y = O, S, Se, C(CN)$_2$ and bis(diselenolene) complexes **[C][AuSeR(=Y)]**, (C = Ph$_4$P$^+$, Et$_4$N$^+$, R = Et, Pr, iPr and Y = S, Se).

The redox properties of the various gold(III) bis(dithiolene) and bis(diselenolene) complexes were investigated by cyclic voltammetry using the same conditions, dichloromethane solutions and NBu$_4$PF$_6$ as supporting electrolyte. The oxidation potentials are shown in Table 1. Under these conditions, the nature of the counter-ion, Ph$_4$P$^+$ or Et$_4$N$^+$, had no influence on the redox properties observed, due to ion exchange with the Bu$_4$N$^+$ of the supporting electrolyte. Thus, only the result of one monoanion is included in Table 1, even if the two salts were analyzed. For all the investigated monoanionic bis(dithiolene) complexes, three redox processes are observed on the cyclic voltammograms. On the anodic scan, the two oxidation waves correspond to the oxidation of the monoanionic species into the neutral and to the monocationic complex. Most of these complexes had the tendency to deposit on the electrode once oxidized and frequently a strong desorption peak was observed on the reversible scan. This phenomenon occurs essentially for the complex with an exocyclic sulfur atom, [AuSR(=S)]$^{-1}$. On the cathodic scan, an irreversible process associated with the reduction in the monoanion into the dianion occurs (Scheme 2). Comparison of the redox potentials shows that when the nature of the side chain was modified from Me, Et, Pr to Bu, no significant differences were observed on the redox potentials. However, the nature of the exocyclic substituent = O, = S, = Se to = C(CN)$_2$ significantly affected the redox potentials. The presence of oxygen instead of sulfur makes the oxidation of the monoanionic into the neutral species easier. On the other hand, the presence of electron-withdrawing substituents such as =C(CN)$_2$ induces an anodic shift of the oxidation potentials by 300 mV, compared with the =O derivative, leading to a monoanion which is more difficult to oxidize than the other complexes of the series. Both derivatives, [AuSEt(=C(CN)$_2$)]$^{-1}$ and [AuSEt(=O)]$^{-1}$ exhibited a wider potential stability window of the neutral species than the sulfur analogues [AuSR(=S)]$^{-1}$ [51]. Indeed, the potential difference between the second and the first oxidation potentials amounts to 470 mV and 410 mV for the =O and the =C(CN)$_2$ derivatives, respectively, while for the =S analogues this value is smaller (170 mV). The gold complexes with selenium atoms, either the bis(dithiolene) with exocyclic selenium atoms or the bis(diselenolene) complexes, exhibited a different behavior, since on the first anodic scan an irreversible oxidation process is observed on the cyclic voltammograms presumably due to strong adsorption phenomenon. For comparison, we also investigated the redox behavior of Auranofin using the same experimental conditions in CH$_2$Cl$_2$ in the presence of NBu$_4$PF$_6$ as a supporting electrolyte. Using these conditions, upon anodic scan only one irreversible oxidation process is observed at 1.42 V vs. SCE.

Therefore, all these monoanionic gold bis(dithiolene) and bis(diselenolene) complexes are easier to oxidize than Auranofin.
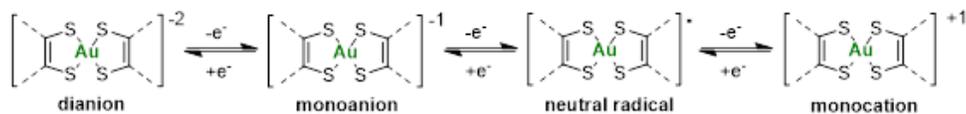
Scheme 2. Representation of the four redox states of gold bis(dithiolene) complexes.

Table 1. Redox potentials of gold bis(dithiolene) and bis(diselenolene) complexes (E in V vs. SCE) in CH_2Cl_2, NBu_4PF_6, Pt, scan rate 100 mV.s^{-1}.

Complexes	$E^{-2/-1}$	$E_{1/2}^{-1/0}$	$E_{pa2}/E_{pc2}^{0/+1}$
[AuSMe(=S)]$^{-1}$	−0.85	0.51/0.44 *	0.73/0.56 *
[AuSEt(=S)]$^{-1}$	−0.90	0.55/0.49 *	0.71/0.61 *
[AuSPr(=S)]$^{-1}$	−0.85 **	0.56/0.53 *	0.73/0.64
[AuSBu(=S)]$^{-1}$	−0.88 **	0.55/0.50	0.75/0.66 *
[AuSEt(=O)]$^{-1}$	−1.05 **	0.42/0.36	0.89/0.83
[AuSEt(=C(CN)$_2$)]$^{-1}$	–	0.71/0.66	1.13/1.06
[AuSeEt(=Se)]$^{-1}$	−0.84 **	0.43/– **	–
[AuSEt(=Se)]$^{-1}$	−0.80 **	0.40/– **	–
[AuSPr(=Se)]$^{-1}$	−0.84 **	0.45/– **	–
[AuSeEt(=S)]$^{-1}$	−0.89 **	0.52/– **	–
[AuSePr(=S)]$^{-1}$	−0.90	0.54/– **	0.95/–
[AuSe*i*Pr(=S)]$^{-1}$	−0.94	0.62/0.57*	0.75/–

* Adsorption; ** Irreversible process.

2.2. Molecular Structure and Intermolecular Interactions in the Solid State

X-ray analyses of novel monoanionic dithiolene complexes [AuSBu(C=S)]$^{-1}$, [AuSEt(=C(CN)$_2$)]$^{-1}$, [AuSEt(=Se)]$^{-1}$ and [AuSPr(=Se)]$^{-1}$, together with monoanionic diselenolene complexes [AuSePr(=S)]$^{-1}$ and [AuSe*i*Pr(=S)]$^{-1}$ have been investigated and the molecular structures of three of these complexes are shown in Figure 1. The molecular structure of the other complexes is presented in Figure S1. All these complexes surrounded by two disymmetric R-thiazdt or R-thiazds ligands are obtained as trans isomers, in the solid state, with a square planar geometry around the gold atom. Besides the [AuSEt(=C(CN)$_2$)]$^{-1}$ complex, all the other monoanionic complexes are not fully planar, as the metallacycles are slightly distorted along the S•••S or Se•••Se axis with dihedral angle in the range of 2 to 6° (see the lateral views of the complexes in Figure 1). The orientation of the chain with alkyl flexible groups, R = Et, Pr, Bu is lateral, while with the bulky isopropyl group R = *i*Pr, the two methyl groups are oriented above and below the plane formed by the complex core.
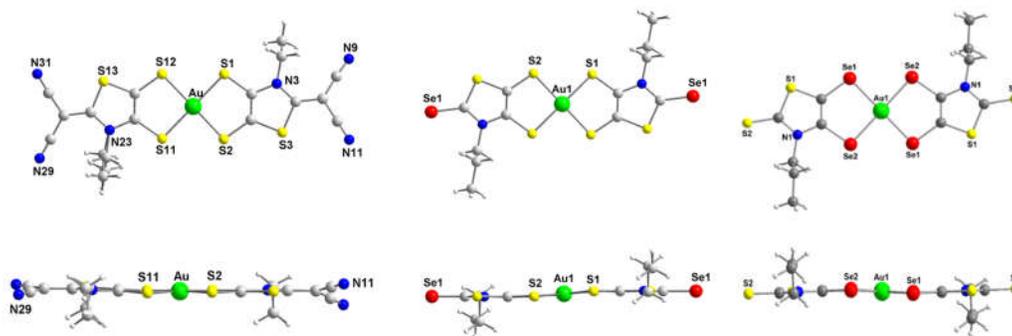
Figure 1. Molecular structures of monoanionic gold complexes, [AuSEt(=C(CN)₂)]⁻¹ (**left**), [AuSPr(=Se)]⁻¹ (**middle**) and [AuSePr(=S)]⁻¹ (**right**).

As these complexes are chalcogen-rich derivatives, in the solid state, various short chalcogen•••chalcogen contacts are observed, shorter than the sum of the van der Waals radii of the involved chalcogen atoms. As a reference, the van der Waals contact distances Se•••Se, S•••Se and S•••S amount to 3.80 Å, 3.70 Å and S•••S 3.60 Å, respectively. The only complex where no short chalcogen•••chalcogen contact was observed is [AuSEt(C=C(CN)₂)]⁻¹. For this complex, hydrogen bonding interactions are established between two neighboring gold complexes involving the nitrogen atoms of one nitrile group and the H of the lateral alkyl chain and between another nitrogen atom of another nitrile group and the H of the counter-ion. In order to exemplify the type of intermolecular chalcogen•••chalcogen short contacts existing in the solid state, the detailed interactions are presented in Figure 2 for the complexes [**P**][AuSePr(=S)] and [**P**][AuSEt(=Se)] and in Figure S2 for [**P**][AuSPr(=Se)] and [**P**][AuSBu(=S)]. Concerning the diselenolene complex [**P**][AuSePr(=S)], the monoanionic gold complexes interact from the longitudinal side of the molecule. For instance, some interatomic distances such as Se•••Se are as short as 3.29 Å and Se1•••S1 3.43 Å, which represent a reduction ratio to 86.6% and 92.7 %, respectively, relative to the van der Waals contact distance (Se•••Se: 3.80 Å, Se•••S: 3.70 Å and S•••S: 3.60 Å).
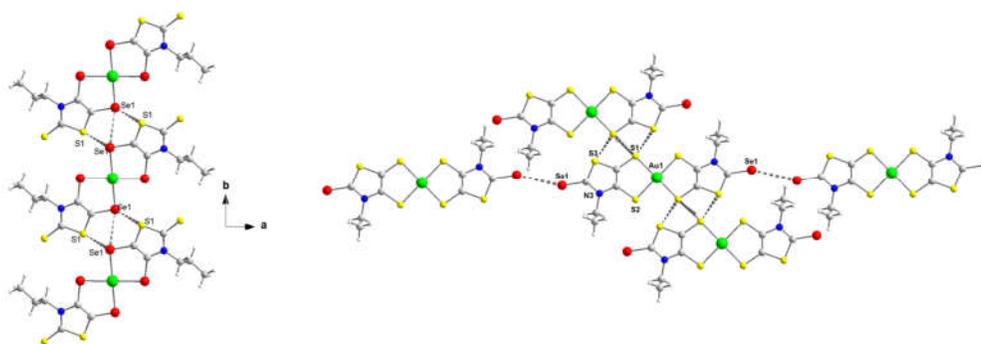
Figure 2. View of the chalcogen•••chalcogen short contacts between neighboring monoanionic gold complexes in [**P**][AuSePr(=S)] (**left**) and [**P**][AuSEt(=Se)] (**right**).

As noticed for the bis(diselenolene) complex [**P**][AuSePr(=S)], the bis(dithiolene) [**P**][AuSEt(C=Se)] forms layers along the ab plane with several short chalcogen••• chalcogen interactions, shorter than twice the van der Waals radii. For example, on the side along the long axis of the molecule, two short S•••S contacts are identified, S1•••S1 3.25 Å and S1•••S3 3.39 Å, which correspond to 90.3 and 94.2 % of the reduction ratio.

Nonetheless, an additional short contact involving the exocyclic selenium atoms is also observed, Se•••Se 3.55Å (RR of 93.4%).

2.3. Cytotoxicity in Ovarian Cells

The anticancer activity of the sixteen complexes under study and the reference drugs Cisplatin and Auranofin was evaluated in the A2780 and OVCAR8 ovarian cancer cells. The Cisplatin-resistant cells OVCAR8 were introduced to ascertain the ability of the complexes to overcome cisplatin resistance, since the majority of ovarian tumors eventually recurs in a drug-resistant form. OVCAR8 were used as a control cell line, selecting the incubation time point of 48 h.

Cells were exposed to increasing concentrations of the complexes (0.01–100 µM) for 24 and/or 48 h, at 37 °C. The IC_{50} values were calculated from dose–response curves using the colorimetric MTT assay. Results show that the differences in the cytotoxic profile were more evident at 24 h incubation, whereas at 48 h incubation most of the complexes displayed similar high cytotoxic activities with IC_{50} values ranging from 0.1–8 µM (A2780) and 0.8–29 µM (OVCAR8). Most complexes presented a similar cytotoxicity profile compared to Auranofin, but higher activity compared to Cisplatin, and, most importantly, were active in the Cisplatin-resistant OVCAR8 cells (Table 2).

Table 2. IC_{50} values (µM) calculated for the sixteen Au(III) bis(dithiolene/diselenolene) complexes and the reference drug Cisplatin and Auranofin on the ovarian cancer cells (A2780 and OVCAR8) after 24 and/or 48 h incubation.
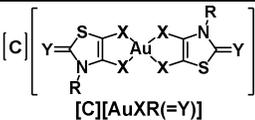
[C][AuXR(=Y)]	IC50 (µM)		
	A2780, 24 h	**A2780, 48 h**	**OVCAR8, 48 h**
[**N**][Au**SMe**(=**S**)]	1.63 ± 0.40	0.11 ± 0.0	2.44 ± 0.78
[**N**][Au**SEt**(=**S**)]	4.23 ± 0.80 *	1.30 ± 0.32 *	3.76 ± 0.71
[**P**][Au**SEt**(=**S**)]	0.58 ± 0.20	0.18 ± 0.0	0.85 ± 0.19
[**P**][Au**SEt**(=**O**)]	0.86 ± 0.11	0.31 ± 0.10	1.16 ± 0.21
[**P**][Au**SEt**(=**Se**)]	0.71 ± 0.12	0.22 ± 0.11	0.97 ± 0.18
[**N**][Au**SEt**(=**C(CN)₂**)]	1.32 ± 0.20	0.17 ± 0.0	1.48 ± 0.41
[**N**][Au**SeEt**(=**S**)]	19.2 ± 2.01	4.32 ± 1.17	29.4 ± 4.20
[**N**][Au**SeEt**(=**Se**)]	26.9 ± 3.02	4.84 ± 1.60	13.9 ± 1.61
[**P**][Au**SeEt**(=**Se**)]	3.96 ± 2.21	0.64 ± 0.19	2.42 ± 1.52
[**N**][Au**SPr**(=**S**)]	2.93 ± 0.81	2.28 ± 0.69	2.28 ± 0.19
[**P**][Au**SPr**(=**S**)]	4.60 ± 1.15 *	0.52 ± 0.23 *	1.04 ± 3.91
[**P**][Au**SPr**(=**Se**)]	0.62 ± 0.19	0.55 ± 0.41	0.80 ± 0.18
[**P**][Au**SePr**(=**S**)]	0.91 ± 0.40	0.29 ± 0.10	1.57 ± 0.43
[**N**][Au**Se*i*Pr**(=**S**)]	30.3 ± 3.39	8.27 ± 1.12	8.76 ± 0.69
[**P**][Au**Se*i*Pr**(=**S**)]	3.74 ± 1.22	0.68 ± 0.18	3.86 ± 0.91
[**P**][Au**SBu**(=**S**)]	1.38 ± 0.28	0.95 ± 0.05	1.41 ± 0.56
Auranofin	2.01 ± 0.71	0.43 ± 0.27 *	1.04 ± 0.41
Cisplatin	21.1 ± 5.0	3.60 ± 1.25 *	10.1 ± 2.3

Results are shown as the means ± SD of two independent experiments carried out with six replicates. * Results from [47].

Interestingly, in relation to their anticancer activity, and when compared at 48 h incubation, these gold complexes clustered in two groups, i.e., those having Ph_4P^+ as a counter-ion and those having Et_4N^+ as a counter-ion, being the former more cytotoxic than the later ones. This is even more obvious when comparing the same gold complexes [N][AuSEt(C=S)] vs. [P][AuSEt(C=S)] (1.30 vs. 0.18), [N][AuSeEt(C=Se)] vs.

[**P**][AuSeEt(C=Se)] (4.84 vs. 0.64), and [**N**][AuSe*i*Pr(C=S)] vs. [**P**][AuSe*i*Pr(C=S)] (8.27 vs. 0.68). Of note, if some discrepancies can be observed after 24 h incubation, the nature of the exocyclic chalcogen atom do not significantly modify the IC$_{50}$ after 48 h incubation for the A2780 ovarian cancer cells. However, for OVCAR8 ovarian cancer cells, the presence of selenium atoms in the metallacycles seems to diminish the efficiency of the gold complexes.

2.4. Toxicity Studies in Zebrafish Embryo

　　Toxicity is a major challenge for drug development and is the leading cause of drug failure. Consequently, the evaluation of the potential toxicity represents a critical step in the development of new drugs. In this context, the zebrafish embryo represents a notable in vivo vertebrate model for studying the toxic effects of chemical compounds due to the small size, robustness, multiple progenies from a single mating, chemical permeability, easiness of observation and maintenance under laboratory conditions. In addition, the close phylogeny of zebrafish and mammals, with highly conserved signaling pathways, makes this species increasingly used and ideal for performing toxicological studies [52–56]. Therefore, we evaluated the complexes acute toxicity by measuring mortality of 72 h post-fertilization (hpf) zebrafish embryos when incubated with increasing concentrations of the Au(III) complexes for 48 h.

　　The zebrafish lethality curves for each complex after 48 h of treatment are presented in Figures S3 and 3 for selected complexes. Complexes were evaluated at concentrations ranging from 0.1–10 μM. For all the investigated complexes having Et$_4$N$^+$ as a counter-ion, the survival was affected upon 24 h of treatment for concentrations higher than 1 μM. Contrariwise, for the complexes with Ph$_4$P$^+$ as counter-ion, no toxicity was evident except for the complex with an exocyclic oxygen atom, [**P**][AuSEt(C=O)]. The nature of the exocyclic atom or group of atoms (=O, =S, or (=C(CN)$_2$) seemed to have an impact on the effect of the gold complexes in the zebrafish embryo model. In fact, [**P**][AuSEt(=O)] was more toxic than [**P**][AuSEt(=S)] (=O vs. =S), and [**N**][AuSEt(=C(CN)$_2$)] was more toxic than [**N**][AuSEt(=S)] (=C(CN)$_2$ vs. =S). Importantly, all the complexes with a Ph$_4$P$^+$ as a counter-ion of formulae [**P**][AuXR(=Y)], with high antitumor effect on cancer cell lines (Table 2), showed low mortality, an interesting property in preclinical studies for novel therapeutic agents.
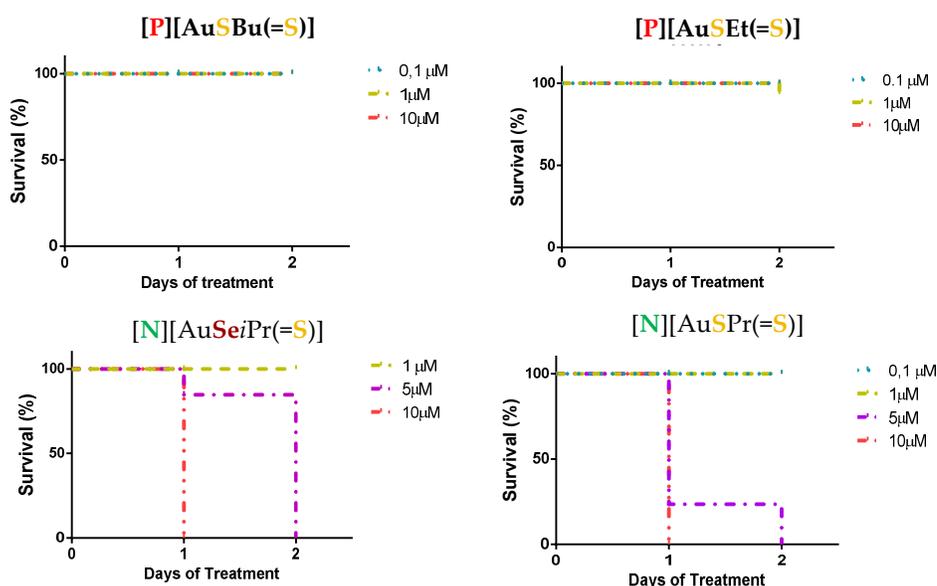

Figure 3. Zebrafish lethality curves of the acute toxicity assay at 48 h for selected Au(III) bis(dithiolene/diselenolene) complexes [**P**][AuSBu(=S)], [**P**][AuSEt(=S)], [**N**][AuSe*i*Pr(=S)] and

[**N**][AuSPr(=S)]. In total, 72 hpf zebrafish embryos (n = 30) were exposed to increased concentrations of the represented complexes and mortality was evaluated after 48 h of treatment with the compounds.

2.5. Antiplasmodial Activity

Au(III) bis(dithiolene/diselenolene) complexes were initially screened for their activity against the obligatory and clinically silent hepatic stage of the rodent *P. berghei* parasite's life cycle (Figure 4). Atovaquone (ATQ), a standard antiplasmodial drug, was employed as a positive control, displaying nanomolar-ranged activity. In the negative control, DMSO was incubated at a percentage equivalent to that of the highest compound concentrations tested. All compounds reduced infection at 5 μM. However, in the case of [**P**][AuSEt(=S)], [**P**][AuSEt(=Se)], [**P**][AuSPr(=Se)], [**N**][AuSMe(=S)], [**P**][AuSEt(=O)] and [**N**][AuSEt(=C(CN)$_2$)], this was accompanied by some degree of toxicity, as observed by the lower cell confluency values. Eight complexes, [**P**][AuSePr(=S)], [**P**][AuSe*i*Pr(=S)], [**P**][AuSEt(=S)], [**P**][AuSEt(=Se)], [**P**][AuSPr(=Se)], [**P**][AuSeEt(=Se)], [**N**][AuSMe(=S)] and [**P**][AuSBu(=S)] presented the strongest activity and were consequently selected for IC$_{50}$ determination (Table 3).
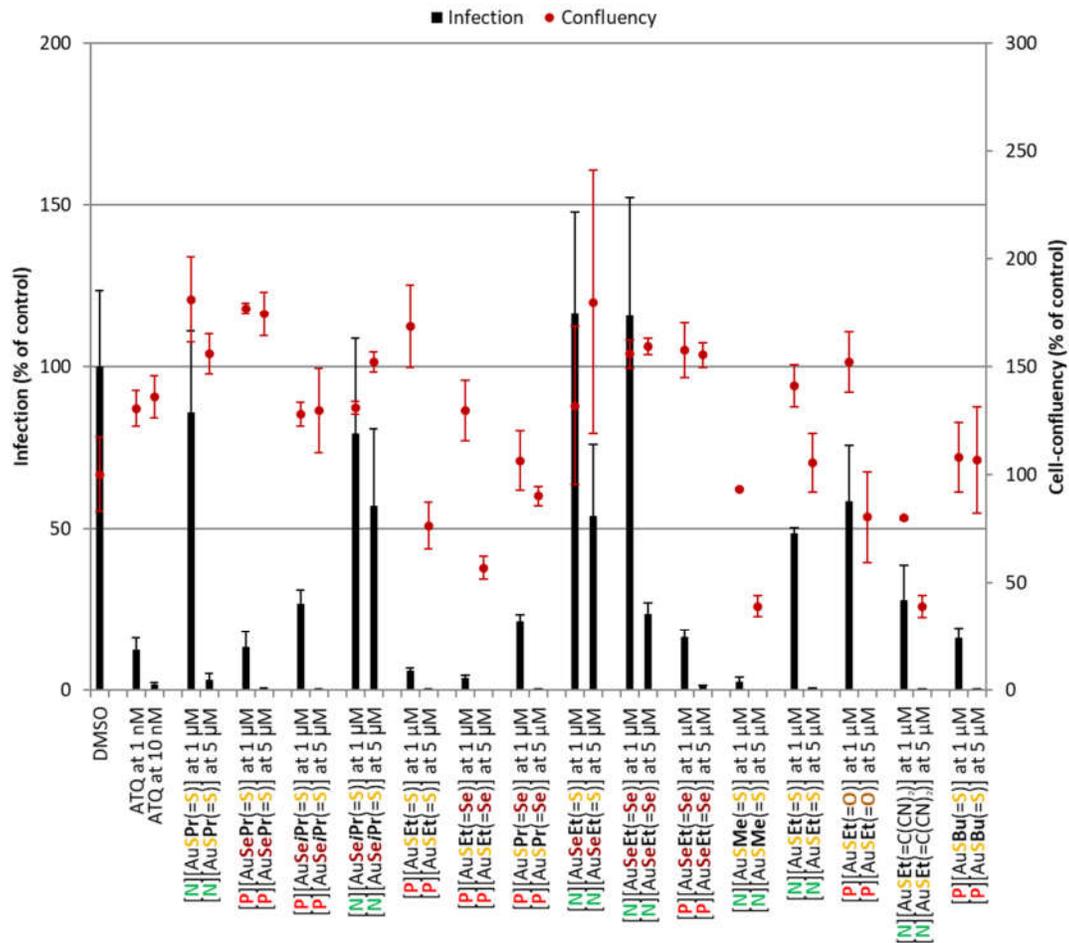

Figure 4. Assessment of the in vitro activity of Au(III) bis(dithiolene/diselenolene) complexes against the hepatic stage of *P. berghei* infection. Total parasite load (infection scale, bars) and cell viability (cell confluency scale, dots) are shown. Results were normalized to the negative control, the drug vehicle DMSO, and are represented as mean ± SD, n = 1. ATQ—Atovaquone.

Complex [**P**][AuSEt(=Se)] was the most active, with an estimated IC$_{50}$ of 415.67 ± 122.73 nM, whereas [**P**][AuSe*i*Pr(=S)] was the least active, with an estimated IC50 of 748.45 ± 70.22 nM. The main difference between these two complexes lies in the nature of the chalcogen within the metallacycle and the exocyclic chalcogen atom. The gold bis(diselenolene) complexes bearing the same exocyclic substituent are less active than the corresponding gold bis(dithiolene) complexes. Among the compounds that presented an interesting liver stage activity, [**P**][AuSEt(=Se)], [**P**][AuSPr(=Se)], [**P**][AuSEt(=S)] and [**P**][AuSBu(=S)] were selected for assessment against the blood stage of *P. falciparum* infection. In this assay, [**P**][AuSEt(=S)] and [**P**][AuSEt(=Se)] displayed the strongest activity against *Pf*NF54 blood stages (Figure 5) and were consequently selected for IC$_{50}$ determination (Table 3).
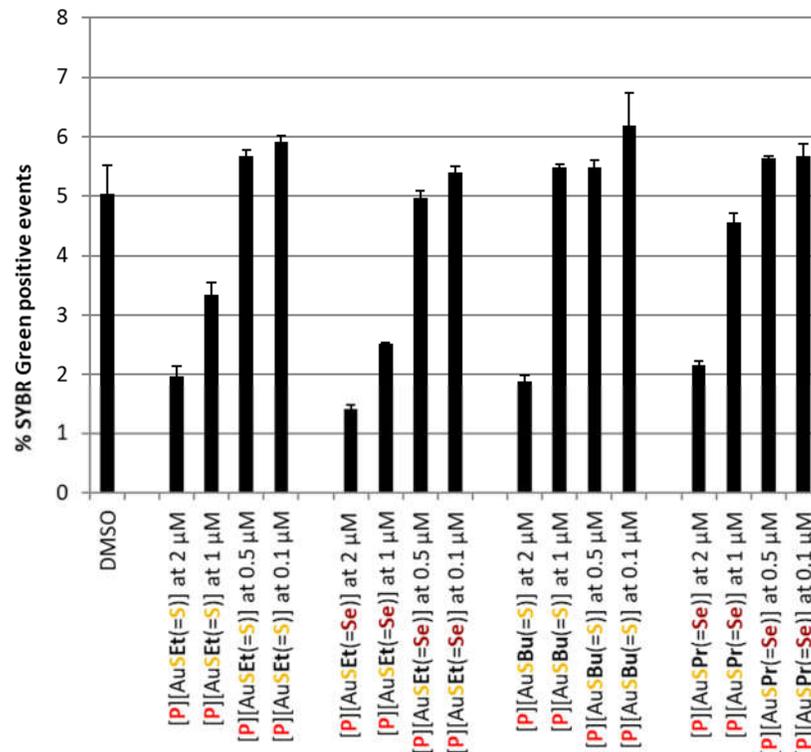
Figure 5. Assessment of the in vitro activity of selected Au(III) bis(dithiolene/diselenolene) complexes against the blood stage of *P. falciparum* NF54 infection. Infection was assessed by flow cytometry as the percentage of SYBR green positive events. A percentage of DMSO equivalent to that present in the highest compound concentrations was employed as a negative control. Results are represented as mean ± SD, n = 1.

Table 3. IC$_{50}$ values of selected Au(III) bis(dithiolene/diselenolene) complexes against the hepatic stage of *P. berghei* and the blood stage of *P. falciparum* NF54 for selected complexes.

	IC$_{50}$ (nM)	
	P. berghei	*Pf*NF54
[**P**][AuSEt(=Se)]	415.67 ± 122.73	1002.30 ± 391.31
[**N**][AuSMe(=S)]	428.73 ± 39.62	ND
[**P**][AuSBu(=S)]	469.57 ± 114.63	ND
[**P**][AuSEt(=S)]	474.00 ± 109.77	1062.25 ± 392.80
[**P**][AuSeEt(=Se)]	517.83 ± 245.87	ND

[**P**][AuSe*i*Pr(=S)]	543.60 ± 19.37	ND
[**P**][AuSPr(=Se)]	643.85 ± 1.34	ND
[**P**][AuSe*i*Pr(=S)]	748.45 ± 70.22	ND

Results are represented as mean ± SD. ND—not determined.

2.6. Antibacterial and Antifungal Activity

The antibacterial activity and antifungal activity of the complexes under study were assessed based on their MIC values against *E. coli*, *S. aureus*, *C. albicans* and *C. glabrata*. Results obtained are presented in Table 4.

All the complexes that demonstrated activity against *S. aureus* have the tetraethylammonium counter-ion Et_4N^+. Interestingly, the same complexes with the tetraphenyl phosphonium counter-ion, Ph_4P^+, are not active, showing again the influence of the counter-ion in the activity of these complexes. Moreover, the nature of the exocyclic substituent also induces some modulation in the activity of the complexes against *S. aureus* as only those with an exocyclic sulfur atom, =S, show minimum inhibitory concentrations. The two complexes exhibiting the closest MIC values to Auranofin (0.2 μg/mL) are the diselenolene gold complex [**N**][AuSe*i*Pr(=S)] (1.5 ± 0.1 μg/mL) and the dithiolene gold complex [**N**][AuSPr(=S)] (1.5 ± 0.1 μg/mL).

Table 4. MIC values (in μg/mL) of the complexes under study against the representative Gram-positive *S. aureus*, the Gram-negative representative *E. coli* and the *Candida* species *C. albicans* and *C. glabrata*. MIC values below 10 μg/mL are boxed in bold.
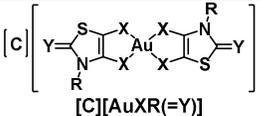
[C][AuXR(=Y)]	MIC (μg/mL)			
	S. aureus **Newman**	*E. coli* **ATCC25922**	*C. albicans* **SC5134**	*C. glabrata* **CBS138**
[**N**][AuSMe(=S)]	4.4 ± 0.2	>250	>62.5 ***	2.9 ± 0.9
[**N**][AuSEt(=S)]*	12.1 ± 3.9	>125	19.9 ± 2.4	9.7 ± 2.7
[**P**][AuSEt(=S)]	>125	>125	>62.5	>62.5
[**P**][AuSEt(=O)]	>125	>125	>62.5	>62.5
[**P**][AuSEt(=Se)]	>125	>125	>62.5	>62.5
[**N**][AuSEt(=C(CN)₂)]	>125	>125	>62.5	>62.5
[**N**][AuSPr(=S)]	1.1 ± 0.2	>250	3.1 ± 0.5	1.6 ± 0.8
[**P**][AuSPr(=S)]**	>125	>125	>125	>125
[**P**][AuSPr(=Se)	>125	>125	62.5	>62.5
[**P**][AuSBu(=S)]	>125	>125	>62.5	>62.5
[**N**][AuSeEt(=S)]	5.5 ± 0.3	>125	>62.5	1.6 ± 0.8
[**N**][AuSe*i*Pr(=S)]	1.5 ± 0.1	>250	>125	2.1 ± 0.1
[**P**][AuSe*i*Pr(=S)]	>62.5	>62.5	>31.25	>31.25
[**P**][AuSePr(=S)]	>250	>250	>125	>125
[**N**][AuSeEt(=Se)]	>62.5	>62.5	>31.25	1.8 ± 0.5
[**P**][AuSeEt(=Se)]	>125	>125	>62.5	>62.5
Auranofin	0.173 ± 0.004	35.5 ± 0.6	7.9 ± 0.5	15.2 ± 0.6

Results are presented as the means ± SD of 3 independent experiments carried out in duplicate. * Complex 1, reference [47]; ** Complex 2, reference [47]; *** Complex precipitates at higher concentrations in RPMIG.

None of the complexes were able to inhibit the growth of *E. coli*. This observation is in line with results obtained previously with gold(III) bis(dithiolene) complexes [46,47].

C. glabrata was the most susceptible to the Au(III) complexes, having its growth affected by six of these complexes, namely [**N**][AuSEt(=S)], [**N**][AuSMe(=S)],

[**N**][AuSeEt(=S)], [**N**][AuSeEt(=Se)], [**N**][AuSPr(=S)] and [**N**][AuSe*i*Pr(=S)]**,** being the MIC value for last five complexes between 1.6 and 2.9 µg/mL. All these active complexes bear the tetraethylammonium counter-ion (Et₄N⁺).

The complex [**N**][AuSPr(=S)] was the most active against *C. albicans*, with a MIC value of 3.1 µg/mL, below the 7.9 µg/mL found for Auranofin.

All the complexes with the tetraphenylphosphonium (Ph₄P⁺) counter-ion were inactive against *S. aureus*, *E. coli*, *C. albicans* and *C. glabrata*.

2.7. Cytotoxicity and Anti-HIV Activity of Auranofin, [P][AuSEt(=S)] and [P][AuSBu(=S)]

No significant cytotoxicity was observed in vitro in TZM-bl culture cells in the presence of [**P**][AuSEt(=S)] and [**P**][AuSBu(=S)] (Figure S4). Auranofin and [**P**][AuSEt(=S)] presented a CC_{50} of 3.21 µM and 4.92 µM, respectively. For [**P**][AuSBu(=S)], it was not possible to calculate the CC_{50} (Figure S4). The activity of Auranofin, [**P**][AuSEt(=S)] and [**P**][AuSBu(=S)] was evaluated in TZM-bl cells in a single-round infectivity assays against HIV-1 SG3.1 reference isolate. Similar to Auranofin, none of the compounds presented anti-HIV-1 activity (Figure 6). Of note, Auranofin was considered a candidate anti-HIV reservoir as it targets the memory T lymphocytes which are the viral reservoirs of HIV-1 [57].
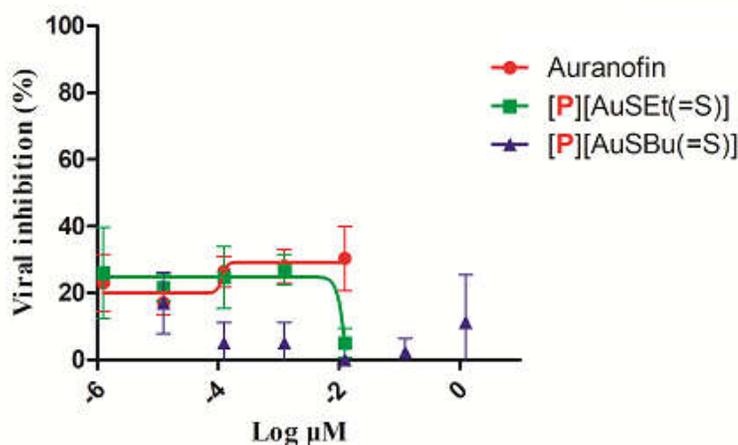

Figure 6. The activity of Auranofin, [**P**][AuSEt(=S)] and [**P**][AuSBu(=S)] in TZM-bl cells in a single-round infectivity assays against SG3.1 HIV-1 reference isolate.

2.8. Mechanistic Studies

The inhibition of thioredoxin reductase (TrxR), the interaction with DNA and the interaction with human serum albumin were assessed for selected complexes to investigate the effect of the substituent on the nitrogen atom of the thiazoline ring, the nature of the exocyclic atom and the counter-ion.

2.8.1. Inhibition of TrxR by the Gold Complexes

The assessment of TrxR as a possible target for antitumor drugs has attracted wide attention as this enzyme participates in the regulation of redox reactions and other important physiological processes, such as cell proliferation, cell differentiation and cell death [58]. Gold complexes typically behave as strong inhibitors of TrxR, possibly due to the high affinity of gold to its active site selenocysteine. Moreover, gold complexes bearing sulfur-containing ligands display stronger association to TrxR [59,60].

The effect of the selected gold complexes on the activity of TrxR was evaluated by a colorimetric DTNB assay as previously described [47]. Figure 7 shows the effect of the complexes tested in a concentration range of 0.1 nM–2 µM, with Auranofin included in

the assay for comparative purposes. As shown in Figures 7 and S5, the inhibitory effect of the complexes differs, although suggesting TrxR as a possible biological target for these complexes. The most active TrxR inhibitors were [**P**][AuSBu(=S)], [**P**][AuSe*i*Pr(=S)] and [**P**][AuSEt(=S)], displaying IC_{50} values of 0.13 ± 0.08 µM, 0.40 ± 0.25 µM and 0.86 ± 0.32 µM, respectively. In contrast, the complex, [**P**][AuSEt(=Se)] with an exocyclic selenium atom was the weaker inhibitor of TrxR, displaying an IC_{50} value of 4.81 ± 1.02 µM. Moreover, it can be noticed that between [**P**][AuSe*i*Pr(=S)] and [**N**][AuSe*i*Pr(=S)], where the only difference is the counter-ion, the weakest effect is with the Et_4N^+, indicating that the nature of the counter-ion has a potential effect on the enzyme. The substituent on the nitrogen atom of the thiazoline ring ([**P**][AuSEt(=S)] vs. [**P**][AuSBu(=S)]) and the nature of the exocyclic atom ([**P**][AuSEt(=S)] vs. [**P**][AuSEt(=Se)]) seemed to influence the inhibitory effect on the enzyme. The exocyclic selenium atoms of [**P**][AuSEt(=Se)] seemed to disfavor the intermolecular interaction with the enzyme in relation with the peripheral thione group of [**P**][AuSEt(=S)]. As expected, Auranofin displayed the lowest IC_{50} value, at least one order of magnitude lower. The TrxR inhibitory potential of these complexes is comparable to that of the $[Au(R\text{-thiazdt})_2]^{-1}$ complexes previously described [47].
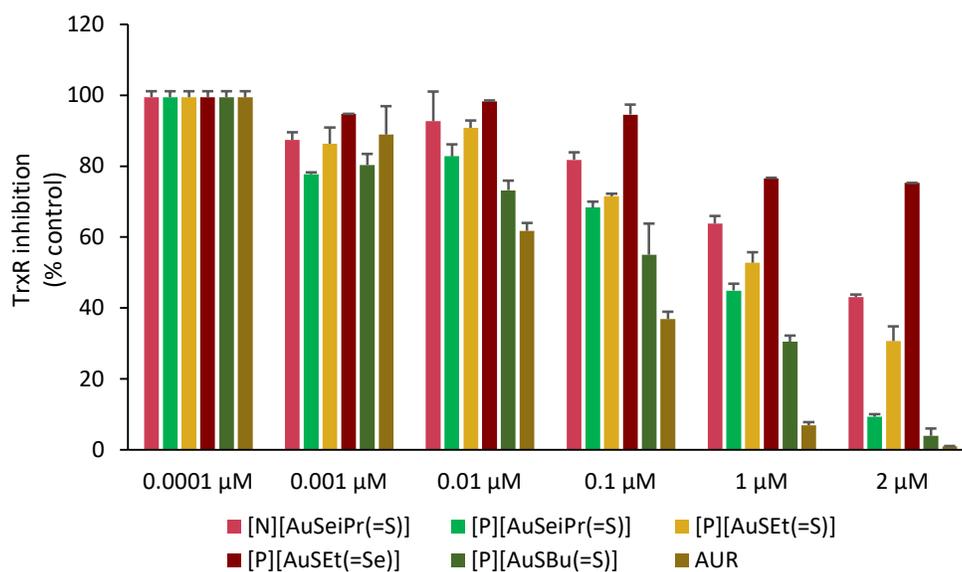

Figure 7. Inhibition of TrxR by the selected complexes under study [**N**][AuSe*i*Pr(=S)], [**P**][AuSe*i*Pr(=S)], [**P**][AuSEt(=S)], [**P**][AuSEt(=Se)], [**P**][AuSBu(=S)] and Auranofin (AUR). Data are shown as the mean ± SD of two independent experiments carried out with four replicates for each complex concentration.

TrxRs from different organisms, such as cells, bacteria and *Plasmodium falciparum*, show different chemical mechanisms of reduction, which constitute the basis for the development of specific TrxR inhibitors against bacterial pathogens and parasitic diseases such as malaria. Most protozoan parasites are fast replicating organisms compared with tumor cells and share the same requirements, i.e., rapid DNA synthesis and protection from ROS generated by the host's immune system. The thioredoxin system can fulfil both tasks and therefore seems to be an essential part of the parasite's metabolism. On the basis of our results, it is likely that most of the complexes impair the antioxidant system of the parasites [61–64]. On the other hand, many Gram-positive and Gram-negative bacteria including *S. aureus* and *E. coli*, respectively, possess the Trx-TrxR system to maintain the thiol-redox balance and also to protect bacterial cells from oxidative stress. However, *E. coli* also has the additional glutathione system to maintain the thiol-redox balance. Auranofin inhibits the bacterial TrxR and impair their redox balance, resulting in bacterial

cell death. In our study, the activities against Gram-positive and Gram-negative bacteria are consistent with other previous reports indicating a high activity against *S. aureus* (MIC = 0.2 μg/mL) and a significant lack of activity for *E. coli.* (MIC = 35.5 μg/mL) [65].

2.8.2. DNA Electrophoresis

Mechanistic studies suggested that, in contrast to Cisplatin, DNA was not the primary target for gold complexes. In fact, gold has different oxidation states, rich coordination chemistry, and therefore, it is possible to tune their biological activities by subtle changes in the structure of the complexes. Gold(III) complexes have been synthesized to reproduce the main features of Cisplatin, i.e., its planar geometry. Unlike Cisplatin, the main biological targets of gold compounds are still unknown. Several reports mention the DNA-independent mechanism of some gold(III) complexes, while others report that binding to DNA is responsible for the cytotoxic effect [16]. We determined the ability of a set of complexes under study to interact with ΦX174 supercoiled DNA in vitro. As shown in Figures 8 and S6, none of the compounds were able to induce conformational changes in the DNA, following the same pattern observed for Auranofin [46]. Cisplatin was able to alter the electrophoretic mobility of the nicked and supercoiled forms of DNA in a dose-dependent way (Figure S6). These results suggest that the cytotoxic effect of these complexes is not mediated by their interaction with the DNA, suggesting instead a mechanism of action distinct from that of Cisplatin.
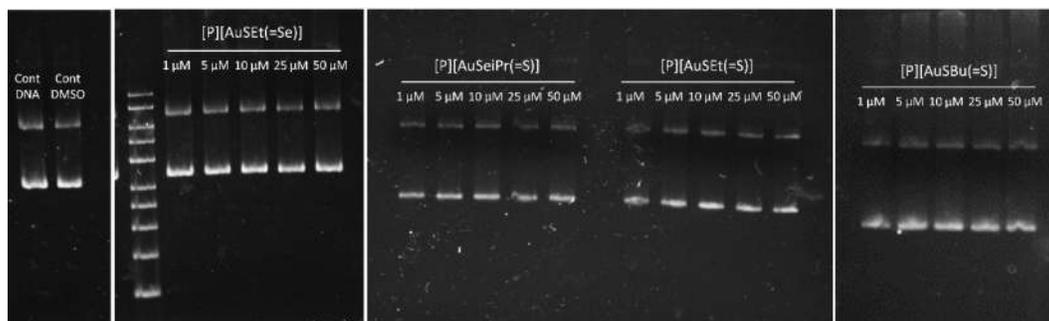

Figure 8. Assessment of the interaction between supercoiled φX174 DNA and selected complexes under study ([**P**][AuSEt(=Se)], [**P**][AuSe*i*Pr(=S)], ([**P**][AuSEt(=S)] and [**P**][AuSBu(=S)],) after 24 h of incubation at 37 °C.

2.8.3. Gold-Complexes–HSA Interaction Studies

Understanding the interaction of a drug with serum proteins is an important aspect to be taken into account in the development of new drugs, since this binding may affect its distribution and transport in the human body, as well as influencing its bioavailability, elimination and toxic effects. Fluorescence spectroscopy was used to investigate the interaction between gold complexes [**P**][AuSEt(=S)], [**P**][AuSEt(=Se)], [**P**][AuSe*i*Pr(=S)] and [**P**][AuSBu(=S)] with HSA, taking advantage of the intrinsic fluorescence of the latter. The complexes display a strong quenching of the intensity of the HSA fluorescence as a function of increasing concentration of gold complexes, indicative of a strong interaction between the Au complexes and this protein, without changes in the emission maximum (Figure 9A–D). Upon incubation of two molar excesses of complexes [**P**][AuSEt(=S)], [**P**][AuSEt(=Se)], [**P**][AuSe*i*Pr(=S)] and [**P**][AuSBu(=S)] with HSA, the fluorescence intensity was quenched by 76.3%, 79.4%, 60% and 89.7%, respectively. No intrinsic fluorescence was observed for the gold compounds, in the range 295–550 nm under our experimental conditions and therefore there is no contribution to the HSA fluorescence.

To gather information about the nature of the interaction of the gold complexes with HSA, the Stern–Volmer relationship was applied (Equation (S2)). As illustrated in the insets of Figure 9A–D, the Stern–Volmer plots for the quenching of HSA by the gold

complexes showed a good linearity within the tested concentrations, indicating that one type of mechanism, dynamic or static, is involved in this process. The binding constants (K_{SV}) deduced from the slope of the linear plot and number of binding sites (n) determined from Eq S3 are presented in Table S1. The K_{SV} values followed the pattern [**P**][AuSBu(=S)] > [**P**][AuSEt(=S)] > [**P**][AuSEt(=Se)] > [**P**][AuSe*i*Pr(=S)]. The bimolecular quenching constants (K_q) estimated from Equation (S2) (Table S1) are much greater than the scattering collision quenching constant (2.0×10^{10} dm^3 mol^{-1} s^{-1}) [66], suggesting that the quenching is mainly due to the formation of ground state complex exclusively and not initiated by the collision/dynamic process.
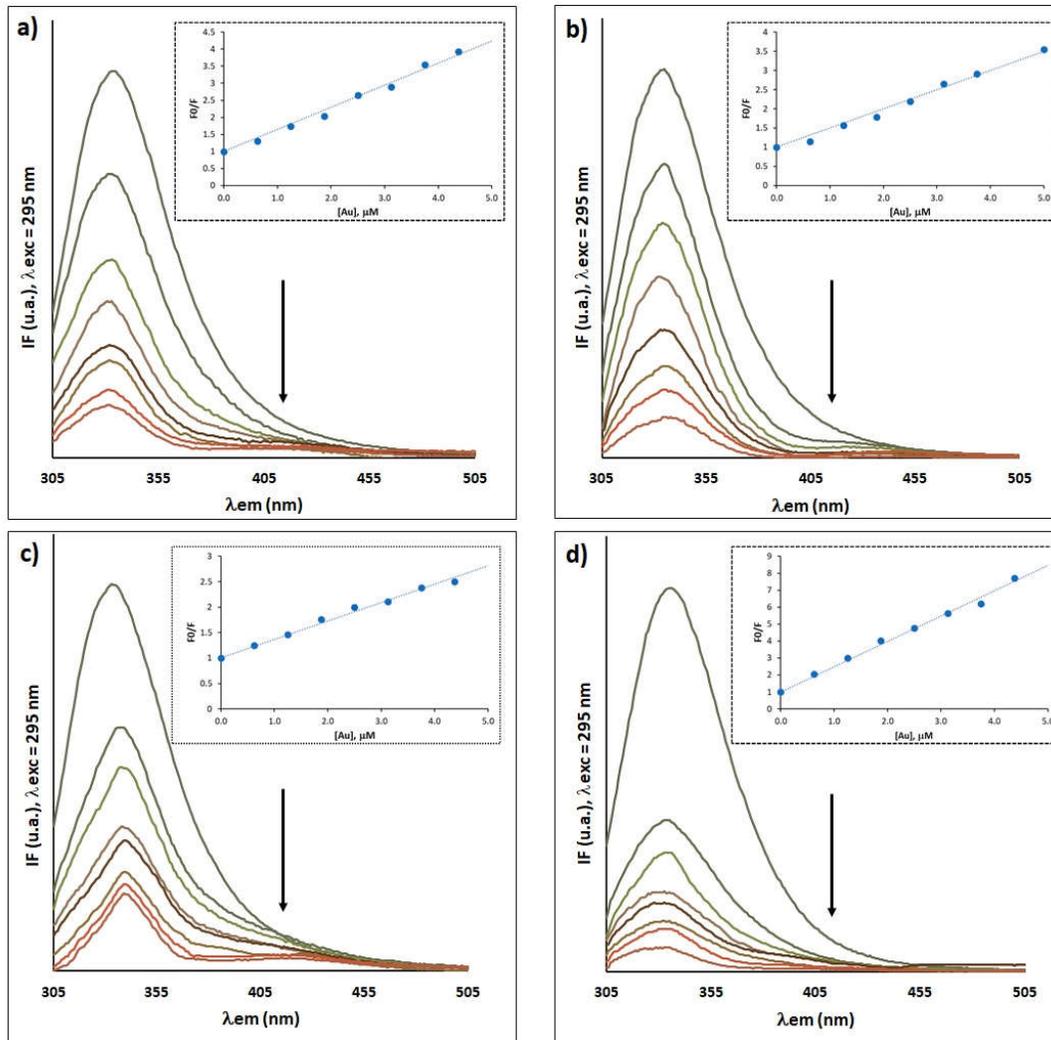
Figure 9. Fluorescence emission spectra in the absence (line with highest IF) and presence of gold complexes: (**a**) [**P**][AuSEt(=S)], (**b**) [**P**][AuSEt(=Se)], (**c**) [**P**][AuSe*i*Pr(=S)] and (**d**) [**P**][AuSBu(=S)]. Inset: Stern–Volmer plot at pH 7.4 of HSA–Au systems. Experimental conditions: [HSA] = 2.5 μM and [gold compound] = 0–5 μM, 10 mM Hepes buffer, pH 7.4; incubation at 37 °C during 24 h.

Overall, the fluorescence spectroscopy indicates that the binding of the gold complexes to the HSA proceeds through a single interaction mode that strongly affects the protein emission, consistent with the formation of a non-fluorescent 1:1 adduct in the ground state for all complexes, except for the complex [**P**][AuSEt(=Se)] which seems to form a non-fluorescent 1:2 adduct. The binding constants determined for these four

complexes are higher than that found for Cisplatin (10^2 M^{-1}) and similar to those found for other gold complexes (10^3–10^4 M^{-1}) [67–71].

3. Materials and Methods

3.1. General Methods for Chemistry

All reagents and materials from commercial sources were used without further purification. NMR spectra were recorded at room temperature using CDCl$_3$ unless otherwise stated (Figures S7–S15). Chemical shifts are reported in ppm and ^{1}H NMR spectra were referenced to residual CHCl$_3$ (7.26 ppm) and ^{13}C NMR spectra were referenced to CHCl$_3$ (77.2 ppm). Mass spectra were recorded with an Agilent 6510 instrument for organics compounds and with a Thermo-Fisher Q-Exactive instrument for complexes by the Center Régional de Mesures Physiques de l'Ouest, Rennes. Cyclic voltammograms (CV)s were carried out on a 10^{-3} M solution of complex in CH$_2$Cl$_2$-[NBu$_4$] [PF$_6$] 0.1 M. CVs were recorded on a Biologic SP-50 instruments at 0.1 Vs^{-1} on a platinum disk electrode. Potentials were measured versus KCl Saturated Calomel Electrode (SCE). Column chromatography was performed using silica gel Merck 60 (70–260 mesh). The solvents were purified and dried by standard methods. The proligand **2-SEt(=C(CN$_2$))**, [72] and complexes [N][AuSMe(=S)], [73] [N][AuSEt(=S)], [74] [P][AuSEt(=O)], [75] [N][AuSeEt(=S)] [75] and [P][AuSPr(=S)] [76] were synthesized according to the previously reported procedure.

3.2. General Synthetic Procedures

3.2.1. Typical Procedure for the Synthesis of the Dithiolene and Diselenolene Proligand 2-XR(=Y):

Under inert atmosphere at 0 °C, lithium diisopropylamide (LDA) was prepared by adding *n*BuLi (2.9 mL, 4.71 mmol, 1.6 M in hexane) to a solution of diisopropylamine (0.7 mL, 4.71 mmol) in 10 mL of anhydrous THF. The LDA solution was added to a solution of **1-R(=Y)** (3.14 mmol) in 40 mL of anhydrous THF at −10 °C. After stirring for 30 min, sulfur for dithiolene or selenium for diselenolene (4.71 mmol) was added to the reaction mixture, and the medium was stirred for an additional 30 min before the addition of LDA (6.28 mmol prepared from 3.9 mL of *n*BuLi, 1.6 M in hexane and 0.9 mL of diisopropylamine in 15 mL of anhydrous THF). The reaction mixture was stirred for 3 h, and sulfur (for dithiolene) or selenium for diselenolene was added (6.28 mmol), followed 30 min later by the addition of 3-bromopropionitrile (2.6 mL, 31.4 mmol). Then, the temperature was allowed to rise to room temperature and the reaction mixture was stirred overnight. Tetrahydrofuran (THF) was evaporated and the residue was extracted with dichloromethane. The organic phase was washed with water and dried over MgSO$_4$. The resulting oil was purified by column chromatography on silica gel using CH$_2$Cl$_2$ as eluent.

2-SBu(=S), brown oil in 59% yield; Rf = 0.45 (SiO$_2$, CH$_2$Cl$_2$); ^{1}H NMR (300 MHz) δ 1.03 (t, 3H, CH$_3$, ^3J = 7.3 Hz), 1.45 (m, 2H, CH$_2$), 1.75 (m, 2H, CH$_2$), 2.75 (t, 4H, CH$_2$, ^3J = 7.0 Hz), 3.14 (t, 2H, CH$_2$, ^3J = 7.0 Hz), 3.20 (t, 2H, CH$_2$, ^3J = 7.0 Hz), 4.39 (t, 2H, CH$_2$, ^3J = 7.3 Hz); ^{13}C NMR (75 MHz) δ 13.7 (CH$_3$), 18.7 (CH$_2$-CN), 19.9 (CH$_2$-CH$_3$), 29.8 (CH$_2$-CH$_2$-N), 31.7 (S-CH$_2$), 32.4 (S-CH$_2$), 49.5 (CH$_2$-N), 117.6 (CN), 117.8 (CN), 125.7 (C=C), 136.1 (C=C), 187.3 (C=S); HRMS (ESI) calcd for C$_{13}$H$_{17}$N$_3$S$_4$$^{+•}$: calcd 343.0305. Found: 343.0335.

2-SePr(=S), beige powder in 51% yield; mp = 142 °C. R$_f$ = 0.54 (SiO$_2$, CH$_2$Cl$_2$/Et$_2$O, 9.8/0.2). ^{1}H NMR (300 MHz) δ 0.99 (t, 3H, CH$_3$, ^3J = 7.5 Hz), 1.76 (sextuplet, 2H, CH$_2$, ^3J = 7.5 Hz), 2.87 (t, 4H, CH$_2$, ^3J = 6.9 Hz), 3.11 (t, 4H, CH$_2$, ^3J = 6.9 Hz), 4.35 (t, 2H, CH$_2$, ^3J = 7.5 Hz). ^{13}C NMR (75 MHz) δ 10.9 (CH$_3$), 19.3 (Se-CH$_2$-CH$_2$-CN), 21.5 (CH$_3$-CH$_2$-CH$_2$-N), 24.2 (Se-CH$_2$-CH$_2$-CN), 52.5 (CH$_3$-CH$_2$-CH$_2$-N), 117.8 (CN), 131.1 (C=C), 188.9 (C=S). HRMS (ASAP) calcd for C$_{12}$H$_{16}$N$_3$S$_2$Se$_2$$^{+•}$: 425.91161, found: 425.9111. Anal. calcd for C$_{12}$H$_{15}$N$_3$S$_2$Se$_2$: C, 34.04; H, 3.57; N, 9.92; S, 15.15. Found: C, 33.90; H, 3.45; N, 9.23; S, 14.87.

2-SeiPr(=S), orange oil in 50 % yield; R$_f$ = 0.43 (SiO$_2$, CH$_2$Cl$_2$/Et$_2$O, 9.8/0.2). Two rotamers can be observed on the NMR spectra. ^{1}H NMR (300 MHz) δ *main rotamer* (56.2%):

1.80 (d, 6H, CH$_3$, ^3J = 7.0 Hz), 3.02 (t, 8H, CH$_2$, ^3J = 7.1 Hz), 5.27 (sept, 1H, CH, ^3J = 7.0 Hz); *other rotamer* (43.8%): 1.64 (d, 6H, 2CH$_3$, ^3J = 7.2 Hz), 2.97 (t, 4H, CH$_2$, ^3J = 7.1 Hz), 3.08 (t, 4H, CH$_2$, ^3J = 7.1 Hz), 5.96 (sept, 1H, CH, ^3J = 7.2 Hz). ^{13}C NMR (75 MHz) δ *main rotamer:* 18.0 (N-CH(CH$_3$)$_2$), 20.2 (Se-CH$_2$-CH$_2$-CN), 25.2 (Se-CH$_2$-CH$_2$-CN), 53.7 (CH), 118.9 (CN), 126.1 (=C), 128.4 (=C), 189.3 (C=S); *other rotamer:* 21.9 (N-CH(CH$_3$)$_2$), 21.2 (Se-CH$_2$-CH$_2$-CN), 27.32 (Se-CH$_2$-CH$_2$-CN), 58.6 (CH), 119.0 (CN), 126.3 (=C), 131.7 (=C), 187.7 (C=S). HRMS (ASAP) calcd for C$_{12}$H$_{15}$N$_3$S$_2$Se$_2$$^{+•}$: 425.91161. Found: 425.9115.

3.2.2. Procedure for the Synthesis of Monoanionic Gold Bis(Dithiolene) and Bis Diselenolene Complexes:

To a dry two-neck flask containing the **2-XR(=Y)** (0.8 mmol), 7.5 mL of 1M solution of sodium methoxide in MeOH was added under nitrogen atmosphere at room temperature. After stirring for 30 min, a solution of potassium tetrachloroaurate (III) hydrate (KAuCl$_4$.H$_2$O) (0.4 mmol) in 7 mL of anhydrous methanol was added to the reaction mixture followed, 5 h later, by the addition of tetraphenylphosphonium chloride Ph$_4$PCl or Et$_4$NBr (0.4 mmol) in 7 mL of anhydrous methanol. The reaction was stirred overnight at room temperature under argon atmosphere. The dark brown solution was filtered over a vacuum flask. The resulting solid was washed with MeOH and recrystallized from acetonitrile.

[P][AuSePr(=S)], black crystals, in 61% yield; mp = 172 °C; ^{1}H NMR (300 MHz) δ 0.97 (t, 6H, CH$_3$, ^3J = 7.5 Hz), 1.77 (m, 4H, CH$_2$, ^3J = 7.6 Hz), 4.05 (t, 4H, CH$_2$, ^3J = 7.6 Hz), 7.61 (m, 8H, CH$_{Ar}$), 7.74 (m, 8H, CH$_{Ar}$), 7.89 (m, 4H, CH$_{Ar}$); ^{13}C NMR (75 MHz) δ (ppm): 11.0 (N-CH$_2$-CH$_2$-CH$_3$), 21.0 (N-CH$_2$-CH$_2$-CH$_3$), 50.2 (N-CH$_2$-CH$_2$-CH$_3$), 104.7 (C=C), 116.5 (C$_{Ar}$), 117.7 (C$_{Ar}$), 128.7 (C=C), 130.5 (C$_{Ar}$), 134.0 (C$_{Ar}$), 135.6 (C$_{Ar}$), 192.6 (C=S); UV-vis-NIR (CH$_2$Cl$_2$) λ (nm), ε (M^{-1}.cm^{-1}): 362, 32455; 314, 27964; 260, 26167; 224, 44491. HRMS (ESI) calcd for [2C$^+$, A$^-$]$^+$ [C$_{60}$H$_{54}$N$_2$P$_2$S$_4$Se$_4$Au]$^+$: 1508.89661, found: 1508.8991. Anal. calcd for C$_{36}$H$_{34}$AuN$_2$PS$_4$Se$_4$: C, 37.06; H,2.94; N, 2.40; S, 10.99. Found: C, 36.59; H, 3.17; N, 2.31; S, 10.69.

[P][AuSe*i*Pr(=S)], black-green crystals, in 48% yield; mp = 216 °C; two rotamers can be observed on the ^{1}H NMR spectrum realized at 243 K the main one at 87% and the other at 13% ^{1}H NMR (300 MHz) δ 1.57 (broad signal, 12H, CH$_3$, 87%), 1.60 (broad signal, 12H, CH$_3$, 13%), 4.56 (broad signal, 2H, CH, 13%), 5.83 (broad signal, 2H, CH, 87%), 7.60 (m, 8H, CH$_{Ar}$), 7.77 (m, 8H, 8CH$_{Ar}$), 7.93 (m, 4H, CH$_{Ar}$). UV-vis-NIR (CH$_2$Cl$_2$) λ (nm), ε (M^{-1}.cm^{-1}): 364, 28982; 318, 32095; 260, 29341; 224, 54311; HRMS (ESI) calcd for calcd for [2C$^+$, A$^-$]$^+$ [C$_{60}$H$_{54}$N$_2$P$_2$S$_4$Se$_4$Au]$^+$: 1508.89661, found: 1508.8976. Anal. calcd for C$_{36}$H$_{34}$AuN$_2$PS$_4$Se$_4$: C, 37.06; H,2.94; N, 2.40; S, 10.99. Found: C, 36.64; H, 3.12; N, 2.38; S, 10.98.

[P][AuSeEt(=Se)], black-green crystals, in 45% yield; mp = 216 °C; ^{1}H NMR (300 MHz) δ 1.33 (t, 6H, CH$_3$, ^3J = 7.2 Hz), 4.28 (q, 4H, CH$_2$, ^3J = 7.2 Hz), 7.60 (m, 8H, CH$_{Ar}$), 7.75 (m, 8H, CH$_{Ar}$), 7.85 (m, 4H, CH$_{Ar}$). HRMS (ESI) calcd for [2C$^+$, A$^-$]$^+$ [C$_{58}$H$_{50}$AuN$_2$P$_2$S$_2$^{80}Se$_6$]$^+$: 1576.7542. Found: 1576.7573. Anal. calcd for C$_{34}$H$_{30}$AuN$_2$PS$_2$Se$_6$. CH$_2$Cl$_2$: C, 31.91; H, 2.45; N, 2.13; S, 4.87. Found: C, 32.08; H, 2.46; N, 2.09; S, 5.21.

[P][AuSEt(=Se)], black-green crystals, in 20% yield; mp = 214 °C; ^{1}H NMR (300 MHz) δ 1.30 (t, 6H, CH$_3$, ^3J = 7.2 Hz), 4.20 (q, 4H, CH$_2$, ^3J = 7.2 Hz), 7.62 (m, 8H, CH$_{Ar}$), 7.78 (m, 8H, CH$_{Ar}$), 7.91 (m, 4H, CH$_{Ar}$); HRMS (ESI) calcd for [2C$^+$, A$^-$]$^+$ [C$_{58}$H$_{50}$AuN$_2$P$_2$S$_6$^{80}Se$_2$]$^+$: 1384.9764. Found: 1384.9776; Anal. calcd for C$_{34}$H$_{30}$AuN$_2$PS$_6$Se$_2$: C, 39.08; H,2.89; N, 2.68. Found: C, 38.77; H, 2.44; N, 2.70.

[N][AuSPr(=S)], black-green crystals, in 47% yield; mp = 231 °C; ^{1}H NMR (300 MHz) δ 0.98 (m, 6H, CH$_3$), 1.32 (m, 12H, CH$_2$), 1.81 (m, 4H, CH$_2$), 3.25 (q, 8H, CH$_2$, ^3J = 7.3 Hz), 4.06 (m, 4H, CH$_2$); HRMS (ESI) calcd for [2C$^+$, A$^-$] [C$_{28}$H$_{54}$AuN$_4$S$_8$]$^+$: 899.17743. Found: 899.1775; Anal. calcd for C$_{20}$H$_{34}$AuN$_3$S$_8$: C, 31.20; H,4.45; N, 5.46. Found: C, 30.87; H, 4.44; N, 5.96.

[P][AuSPr(=Se)], black-green crystals, in 47% yield; mp = 228 °C; ^{1}H NMR (300 MHz) δ 0.96 (m, 6H, CH$_3$), 1.79 (m, 4H, CH$_2$), 4.09 (m, 4H, CH$_2$), 7.61 (m, 8H, CH$_{Ar}$), 7.76 (m, 8H,

CH$_{Ar}$), 7.89 (m, 4H, CH$_{Ar}$); HRMS (ESI) calcd for [2C+A$^-$] [C$_{12}$H$_{14}$AuN$_2$S$_6$^{80}Se$_2$]$^-$: 734.4828. Found: 734.7488. Anal. calcd for C$_{36}$H$_{34}$AuN$_2$PS$_6$Se$_2$: C, 40.30; H,3.19; N, 2.61. Found: C, 40.24; H, 3.44; N, 2.96.

[P][AuSBu(=S)], dark crystals, in 29 % yield. mp 225 °C ;^{1}H NMR (300MHz, (CD$_3$CN) δ 0.95 (t, 6H, CH$_3$, ^{3}J = 7.3 Hz), 1.39 (sext, 4H, CH$_2$, ^{3}J = 7.3 Hz), 1.70 (m, 4H, CH$_2$), 4.06 (t, 4H, CH$_2$, ^{3}J = 7.3 Hz), 7.69 (m, 16H, Ar), 7.91 (m, 4H, Ar); ^{13}C NMR (75 MHz, (CD$_3$)$_2$SO) δ 13.5 (CH$_3$), 19.5 (C̲H$_2$-CH$_3$), 29.1 (C̲H$_2$-CH$_2$-CH$_3$), 46.9 (CH$_2$-N), 110.2 (C = C), 117.1 (C$_{Ar}$), 118.3 (C$_{Ar}$), 130.4 (C$_{Ar}$), 134.6 (C$_{Ar}$), 135.4 (C = C), 190.7 (C = S); Anal. calcd for C$_{38}$H$_{38}$AuN$_2$PS$_8$: C, 45.32; H, 3.80; N, 2.78; S, 25.47. Found: C, 45.47; H, 3.92; N, 2.72; S 24.97.

[N][AuSEt(=C(CN)$_2$)], 47% yield as dark crystals; Mp > 250 °C**;** ^{1}H NMR (300 MHz, (CD$_3$)$_2$SO) δ 1.18 (m, 12H, CH$_3$), 1.31 (t, 6H, CH$_3$, ^{3}J = 7.1 Hz), 3.21 (q, 8H, CH$_2$, ^{3}J = 7.3 Hz), 4.07 (q, 4H, CH$_2$, ^{3}J = 7.1 Hz); ^{13}C NMR (75 MHz, (CD$_3$)$_2$SO) δ 7.6 (N-(CH$_2$-C̲H$_3$)$_4$), 15.0 (N-CH$_2$-C̲H$_3$), 44.6 (N-CH$_2$), 51.9 (N-(C̲H$_2$-CH$_3$)$_4$) 111.0 (C̲-CN), 117.3 (C = C), 134.3 (CN), 174.3 (C̲ = C(CN)$_2$). HRMS (ESI) calcd for [2C$^+$, A$^-$]$^+$ [C$_{32}$H$_{50}$N$_8$S$_6$Au]$^+$: 935.21428. Found: 935.2143. Anal. calcd for C$_{24}$H$_{30}$AuN$_7$S$_6$ .CH$_2$Cl$_2$: C, 33.71; H 3.62; N, 11.01; S, 21.59. Found: C, 33.24; H, 3.58; N, N, 10.76; S, 21.85.

[P][AuSEt(=C(CN)$_2$)], 40% yield as dark crystals; Mp > 250 °C; ^{1}H NMR (300 MHz, CD$_3$CN) δ 1.34 (t, 6H, CH$_3$, ^{3}J = 7.3 Hz), 4.10 (q, 4H, CH$_3$, ^{3}J = 7.3 Hz), 7.70 (m, 16H, Ar), 7.91 (m, 4H, Ar); ^{13}C NMR (75 MHz, (CD$_3$)$_2$SO) δ 14.9 (CH$_3$), 44.3 (CH$_2$), 112.1 (C̲-CN), 117.0 (C = C), 117.5 (C = C), 118.2 (CN), 130.4 (C$_{Ar}$), 134.4 (C$_{Ar}$), 136.1 (C$_{Ar}$), 174.7 (C̲ = C(CN)$_2$); HRMS (ESI) calcd for [2C$^+$, A$^-$]$^+$ [C$_{64}$H$_{50}$P$_2$S$_6$Au]$^+$: 1353.15566. Found: 1353.1551. Anal. calcd for C$_{40}$H$_{30}$AuN$_6$PS$_6$ +2CH$_2$Cl$_2$: C, 42.58; H 2.89; N, 7.09. Found: C, 42.44; H, 2.86; N, 7.10.

3.3. Crystallography

Data collections were performed on an APEXII Bruker-AXS diffractometer equipped with a CCD camera for [P][AuSePr(=S)], [P][AuSeiPr(=S)], [P][AuSEt(=Se)], [P][AuSPr(=Se)], [P][AuSBu(=S)], on a D8 VENTURE Bruker AXS diffractometer for [P][AuSEt(=C(CN)$_2$)]. Apart from [P][AuSEt(=C(CN)$_2$)], the structures were solved either by direct methods using the *SIR97* program [77] and then refined with full-matrix least-square methods based on *F*^{2} (*SHELXL-97*) [78] with the aid of the *WINGX* [79] program. For [P][AuSEt(=C(CN)$_2$)], the structure was solved by direct methods using SIR97 program [77], and then refined with full-matrix least-squares methods based on F^2 (SHELXL program [80]). All non-hydrogen atoms were refined with anisotropic atomic displacement parameters. H atoms were finally included in their calculated positions. Details of the final refinements are summarized in Table S2 in supporting information.

3.4. Biological Studies

3.4.1. Cytotoxic Activity

The cytotoxic activity of the complexes was evaluated in the A2780 (cisplatin sensitive) (Sigma-Aldrich) and OVCAR8 (cisplatin resistant) (ATCC) ovarian cancer cells. Cells were grown in RPMI-1640 medium (Gibco, Thermo Fisher) supplemented with 10% fetal bovine serum (FBS) and were maintained at 37 °C in a humidified atmosphere with 5% CO$_2$. The complexes were initially dissolved in DMSO and then in culture medium to prepare serial dilutions in the range 10^{-9}–10^{-4} M. After 24 and/or 48 h incubation the cellular viability was measured by the colorimetric MTT assay, as previously described [46,47].

The in vitro cytotoxicity of auranofin, [P][AuSBu(=S)] and [P][AuSEt(=S)] was evaluated in TZM-bl cells using alamarBlue cell viability reagent (Life Technologies, USA) [81]. TZM-bl cells (AIDS Research and Reference Reagent Program, National Institutes of Health, USA) were cultured in complete growth medium that consists of Dulbecco's minimal essential medium (DMEM) supplemented with 10% fetal bovine serum (FBS), 100 U/ml of penicillin-streptomycin (Gibco/Invitrogen, Waltham, MA, USA), 1 mM of sodium pyruvate (Gibco/Invitrogen, USA), 2 mM of L-glutamine (Gibco/Invitrogen, USA)

and 1 mM of non-essential amino acids (Gibco/Invitrogen, USA). Cells were cultured in the presence and absence of serial-fold dilutions of the compounds. At least two independent experiments were performed for each cytotoxicity analysis. Each dilution of each compound was performed in triplicate wells. For each assay we had medium controls (only growth medium), cell controls (cells without test compound) and cytotoxicity controls (a compound that kill cells). The cytotoxicity of each compound was expressed by the 50% cytotoxic concentration (CC_{50}), which is the concentration of compound causing 50% decrease in cellular viability.

3.4.2. Toxicological Assessment in Zebrafish Embryo

To test the toxicological effect of the gold (III) complexes, zebrafish (*Danio rerio*) embryos at developmental stage of 72 h post-fertilization (hpf) were exposed to different concentrations of the target complexes and mortality was assessed for 48 h of treatment. Thus, the incubation of a total of 30 embryos per compound concentration was carried in 6-well plates (5 embryos per well) in zebrafish embryo medium (14 mM NaCl, 0.5 mM KCl, 0.02 mM Na_2HPO_4, 0.04 mM KH_2PO_4, 1.36 mM $CaCl_2$, 2.13 mM $MgSO_4$, 4.34 mM $NaHCO_3$, prepared in 100 mL dH_2O). Concentrations used for each compound varied between 0.1 and 10 μM, as described below. The incubation medium was daily renewed. Control DMSO concentration was used as the highest concentration of each gold (III) compound.

3.4.3. In Vitro Activity of Gold Complexes against the Hepatic Stage of *P. berghei* Infection

The in vitro liver stage activity of gold complexes was assessed against *P. berghei*-infected Huh7 cells, as previously described [47,82]. Briefly, Huh7 cells were cultured in RPMI-1640 medium supplemented with 10% (v/v) fetal bovine serum, 1% (v/v) penicillin/streptomycin, 1% (v/v) glutamine, 1% (v/v) non-essential amino acids and 10 mM HEPES. On the day prior to infection, Huh7 cells were seeded in 96-well plates at a density of approximately 3.1×10^4 cell/cm^2 and incubated at 37 °C, 5% CO_2. Stock solutions of the complexes were initially prepared in DMSO and serially diluted in infection medium, i.e., culture medium supplemented with gentamicin (50 μg/mL) and fungizone (0.8 μg/mL), to obtain the test concentrations. As a control, DMSO was diluted in infection medium to a percentage that equals that of the highest compound concentrations tested. These dilutions were added to the cells in triplicates and incubated for 1 h at 37 °C, 5% CO_2, after which 1×10^4 luciferase-expressing *P. berghei* sporozoites were added to each well. Plates were centrifuged at 1800× *g* for 5 min at room temperature and incubated for the duration of the assay. At 46 hours post-infection (hpi), the impact of each compound concentration on cell viability was assessed by the Alamar Blue (Invitrogen, UK) assay, according to the manufacturer's recommendations. Infection was next assessed by bioluminescence, employing the Firefly Luciferase Assay Kit 2.0 (Biotium, USA), according to the manufacturer's recommendations. For IC50 determination, nonlinear regression analysis was employed to fit the normalized results of the dose–response curves, using GraphPad Prism 8 (GraphPad software, La Jolla, CA, USA).

3.4.4. In Vitro Activity of Gold Complexes against the Blood Stage of *P. falciparum* Infection

Ring-stage synchronized cultures of *Pf*NF54 at 2.5% hematocrit and at approximately 1% parasitemia were incubated with gold complexes or DMSO (vehicle control) in 96 well-plates, for 48 h, at 37 °C in a 5% CO_2 and 5% O_2 atmosphere. Stock solutions of Chloroquine (positive control), [**P**][AuSEt(=S)] and [**P**][AuSEt(=Se)] were prepared in DMSO. Working solutions were prepared from the stock solutions in complete malaria culture medium (CMCM), which consists of RPMI 1640 supplemented with 25 mM HEPES, 2.4 mM L-glutamine, 50 μg/mL gentamicin, 0.5% w/v Albumax, 11 mM glucose, 1.47 mM

hypoxanthine and 37.3 mM NaHCO$_3$. For each measurement, 5 µL of the culture (approximately 800,000 cells) was stained with the DNA-specific dye SYBR green I at 1×. After 20 min of incubation, in the dark, the stained sample was analyzed by flow cytometry. For each flow cytometric measurement, approximately 100,000 events were analyzed. All samples were analyzed in triplicate and two independent experiments were performed.

3.4.5. Bacterial and Fungal Strains

The bacterial strains *Escherichia coli* ATCC25922 and *Staphylococcus aureus* Newman were used in this work and maintained in Lennox Broth (LB) solid medium, composed of 10 g/L tryptone, 5 g/L yeast extract, 5 g/L NaCl and 20 g/L agar. The fungal strains *Candida albicans* SC5134 and *C. glabrata* CBS138 were used in this work and maintained in YPD solid medium, composed of 20 g/L glucose, 20 g/L peptone, 10 g/L yeast extract and 15 g/L agar. The strains were isolated from human infections [83–86].

3.4.6. Antimicrobial Activity

The antimicrobial activity of the complexes towards the bacterial and fungal strains was assessed by the determination of the Minimal Inhibitory Concentration (MIC) of each complex towards the indicated microbial strains, based on standard methods, and as previously described [47,87,88]. Briefly, stock solutions of the complexes were prepared in 100% DMSO at final concentrations of 10 mg/mL (complexes [**N**][AuSPr(=S)], [**P**][AuSePr(=S)], [**N**][AuSe*i*Pr(=S)] and [**N**][AuSMe(=S)]), 5 mg/mL (complexes [**P**][AuSEt(=S)], [**P**][AuSEt(=Se)], [**P**][AuSPr(=Se)], [**N**][AuSeEt(=S)]Y1, [**P**][AuSeEt(=Se)], [**P**][AuSEt(=O)], [**N**][AuSEt(=S)], [**N**][AuSEt(=C(CN)$_2$)], [**P**][AuSBu(=S)] and Auranofin) or 2.5 mg/mL (complexes [**P**][AuSe*i*Pr(=S)] and [**N**][AuSeEt(=Se)]), depending on the solubility of each complex. Serial 1:2 dilutions of stock solutions were prepared for each complex in Mueller–Hinton (MH) broth (Fluka Analytical) or RPMI-1640 medium (Sigma) supplemented with 20 g/L glucose and buffered with 0.165 M morpholinepropanesulphonic acid (RPMIG) to pH 7.0. Solutions prepared with MH were used for testing bacteria, while those prepared with RPMIG were used for testing fungi. For antibacterial activity assays, the final concentrations ranged from 250 to 0.24 µg/mL (when stock solution final concentration was 10 mg/mL), 125 µg/mL to 0.12 µg/mL (when stock solution final concentration was 5 mg/mL) and 62.5 to 0.06 µg/mL (when stock solution final concentration was 2.5 mg/mL). For antifungal assays, the final concentrations ranged from 125 µg/mL to 0.12 µg/mL (when stock solution final concentration was 10 mg/mL), 62.5 to 0.06 µg/mL (when stock solution final concentration was 5 mg/mL) and 31.25 to 0.03 µg/mL (when stock solution final concentration was 2.5 mg/mL). Then, 100 µL aliquots of adequately diluted bacterial suspensions of *S. aureus* Newman or *E. coli* ATCC 25922 were mixed with the MH serially diluted complexes aliquots to obtain 5×10^5 CFU/mL. In the case of fungi, cultures were diluted to obtain a final optical density of 0.025, measured at 530 nm (OD$_{530}$). Bacterial suspensions were prepared from cultures grown for 5 h in MH broth at 37 °C and 250 rev·min^{-1} and adequately diluted with fresh MH medium, while fungal suspensions were prepared from overnight cultures grown in YPD broth at 30 °C and 250 rev.min^{-1} and diluted in buffered RPMIG. After 22 h of incubation at 37 °C (bacteria) or 24 h at 35 °C (fungi), the wells' content was resuspended by pipetting and the OD$_{640}$ (bacteria) or OD$_{530}$ (fungi) were measured in a SPECTROstar Nano microplate reader (BMG Labtech).

At least three independent experiments were performed in duplicate for each complex under study. MIC values were estimated after fitting the OD mean values measured for bacteria and fungi after 24 h of incubation, using a modified Gompertz equation and the GraphPad Prism software (version 6.07) [89]. Positive (no complex) and negative controls (no inoculum) were performed for each experiment. The effect of 5% (V/V) DMSO on microbial growth was also assessed.

3.4.7. Anti-HIV Assays

The HIV-1 SG3.1 subtype B strain was obtained by transfection of HEK293T cells with pSG3.1 plasmid using jetPrime transfection reagent (Polyplus-tranfection SA, Illkirch, France) according to the manufacturer's instructions. The 50% tissue culture infectious dose ($TCID_{50}$) of the virus was determined in a single-round viral infectivity assay using a luciferase reporter gene assay [90] in TZM-bl cells and calculated using the statistical method of Reed and Muench [91].

The antiviral activity of Auranofin, [**P**][AuSEt(=S)] and [**P**][AuSBu(=S)] compounds was determined in a single-round viral infectivity assay using TZM-bl reporter cells, as previously described [90]. Briefly, TZM-bl cells were infected with 200 $TCID_{50}$ of SG3.1 in the presence of serial fold dilutions of the compounds in growth medium, supplemented with DEAE-dextran. After 48 h of infection, luciferase expression was quantified with Pierce Firefly Luc One-Step Glow Assay Kit (ThermoFisher Scientific, Rockford, USA) according to the manufacturer's instructions.

At least two independent experiments were performed for each antiviral activity analysis. The assay was set up in triplicate wells. Virus controls and cell controls were used.

3.5. Mechanistic Studies for Relevant Complexes

3.5.1. DNA

The potential interaction of the complexes with DNA was evaluated through the assessment of the electrophoretic mobility of supercoiled ϕX174 DNA, using a previously described method [46]. To that end, a mixture was prepared containing 200 ng of supercoiled ϕX174 DNA (Promega) in 10 mM of phosphate buffer (pH 7.2) and increasing concentrations of Cisplatin, as a positive control, or the metal complexes (in a total volume of 20 μL). The mixture was incubated for 24 h at 37 °C, in the dark. As controls, samples having non-incubated plasmid and plasmid incubated with DMSO were also prepared. Then, all samples were prepared for electrophoresis through the addition of 2 μL of 10× DNA loading buffer (Applichem) and loading on an 0.8% agarose gel in TBE buffer (Thermo Fisher Scientific). The gel was run at 90 V for approximately 3 h, stained using a 3× GelRed® (Biotium) solution in H_2O, and the bands visualized using an AlphaImagerEP (Alpha Innotech) under UV light.

3.5.2. Thioredoxin (TrxR) Inhibition Study

The thioredoxin (TrxR) inhibition assays were performed using a commercial kit from Sigma-Aldrich, introducing minor modifications for a 96-well plate format. The assay is based on the reduction of DTNB (5,5′ dithiobis(2-nitrobenzoic acid)) into TNB (5-thio-2-nitrobenzoic acid) with the concomitant oxidation of NADPH, in a reaction catalyzed by TrxR [92]. The complexes were dissolved in DMSO to prepare serial concentrations in the range of 0.1 nM–2 μM. The reaction mixture (200 μL total volume) contained 11 μL assay buffer (phosphate buffer, pH 7.0 and 50 mM EDTA), 180 μL working buffer (phosphate buffer and 0.25 mM NADPH), 1 μL complexes' solutions, 2 μL enzyme solution and 6 μL DTNB (0.1 M in DMSO). A blank sample (no enzyme) and a positive control (no complexes) were included in the assays. The formation of TNB was monitored at 412 nm with a plate spectrophotometer (Power Wave Xs, Bio-Tek).

3.5.3. HSA-Binding Experiments

Sample Preparation for Spectrofluorometric Experiments

Stock solutions of HSA were prepared by dissolving HSA in 10 mM Hepes buffer, pH 7.4. The protein concentration was determined spectrophotometrically using the molar absorption coefficient of 36,500 M^{-1} cm^{-1} at 280 nm [93]. The complexes [**P**][AuSEt(=S)], [**P**][AuSEt(=Se)], [**P**][AuSe*i*Pr(=S)] and [**P**][AuSBu(=S)] were first prepared at 1 mM concentration in DMSO due to the limited solubility of the complexes in aqueous

media. A series of complex–protein solutions were prepared by adding different concentrations of gold complexes solutions to the protein solution previously prepared. After preparation of the batch complex–protein solutions, the final concentration of DMSO was 1%. For fluorescence acquisition, the final HSA concentration was 2.5 mM and the gold concentrations were 0, 0.6, 1.3, 1.9, 2.5, 3.1, 3.8, 4.4 and 5 mM. The mixtures were stirred to ensure the formation of a homogeneous solution and then kept in an incubator at 37 °C for 24 h in the dark to stabilize and enhance the interaction time. The reference solutions without protein were prepared following the procedures described above.

Fluorescence Spectroscopic Measurements

Steady-state fluorescence measurements were performed with a Fluorolog Model-3.22 spectrofluorimeter from Horiba Jobin Yvon at 25 °C. All the experiments were performed in Hellma® semi-micro fluorescence cuvettes (Suprasil® quartz, path-length 10 × 4 mm, chamber volume 1.4 μL) with the 10 mm path length for the excitation of the sample. The excitation and emission bandwidths were fixed at 4.0 nm, and the excitation wavelength was 295 nm to excite selectively the tryptophan 214 residue, the emission spectra were recorded from 305 to 550 nm. Buffer solutions of gold complexes in corresponding concentrations were used as reference for the measured fluorescence spectra of protein–complex mixtures. The fluorescence intensities were corrected for the absorption of the exciting light and reabsorption of the emitted light to decrease the inner filter effect [94,95] using UV–visible absorption data recorded for each sample on a Jasco V-660 spectrophotometer in the range of 260 to 800 nm with 1 mm path quartz cells. More details and all the equations can be found in the SI.

4. Conclusions

In the present study, sixteen structurally related monoanionic gold(III) bis(dithiolene/diselenolene) complexes were synthesized and characterized by standard analytical techniques. These gold(III) complexes with dithiolene ligands are redox-active molecules which are known as excellent precursors of molecular materials exhibiting conducting properties. Within this study we explored the prospective pharmacological use of these gold complexes, namely as anticancer, antiplasmodial, antibacterial, antifungal and anti-HIV agents. These complexes feature square planar geometries, such as Cisplatin. Based on the molecular structure, a similar mechanism of action, e.g., interaction with DNA, would be expected for these complexes. Reports on the biological activity of similar gold(III) complexes are relatively scarce in the literature. Moreover, these complexes are monoanionic, which in theory do not favor their uptake into cells due to the negatively charged plasma membrane. In this regard, studies on the mechanism of uptake of prospective metal drugs are relatively rare and, similar to Cisplatin, the uptake usually occurs by more than one mechanism.

Cisplatin and Auranofin were included in this study as positive controls. The mode of action of Cisplatin relies on the binding to nuclear DNA, interfering with normal transcription and/or DNA replication mechanisms. Several targets have been proposed to be involved in the action of Cisplatin. In fact, before reaching the target DNA, many other cellular biomolecules such as sulfur-containing glutathione and metallothionein can be targeted and deactivated. The main mechanism of action of Auranofin is through the inhibition of redox enzymes such as TrxR. The overexpression of TrxR is associated with aggressive tumor progression and poor survival in patients with several types of cancers. The thiol group in Auranofin structure has a high affinity to bind thiol and selenol groups of proteins, thus forming stable and irreversible adducts. Redox enzymes such as TrxR are essential to many cellular processes, particularly in maintaining the intracellular levels of reactive oxygen species (ROS) to prevent the resulting DNA damage. An alternative mechanism of action of Auranofin is through the inhibition of the ubiquitin–proteasome system in cancer cells, which are involved in cell cycle regulation, protein degradation, gene expression and DNA repair.

Most of the gold complexes herein exhibited strong anticancer activities similar to Auranofin. However, regarding the antiplasmodial, antibacterial and antifungal activities, most of the complexes displayed selective activities, i.e., those that present outstanding cytotoxic activities also display high antiplasmodial activities, which contrasts with their antibacterial and antifungal properties. Complexes′ features, in particular the counter-ion and the nature of the exocyclic atom or group of atoms, seemed to be relevant for their biological activities. Similar to Auranofin, the complexes failed to interact with ΦX174 supercoiled DNA, indicating that DNA is not their cellular target. In contrast, complexes were able to interact with TrxR and inhibit its activity, although to a lesser extent than Auranofin. HSA could be a possible vehicle of transport for these gold complexes due to their strong affinities for the protein. This result constitutes an interesting finding, as the therapeutic value of a prospective drug is dependent on its availability at the target site. The mode of binding to albumin is central to understanding the pharmacokinetic profile and has a major influence on the therapeutic efficacy.

In this contribution, the main findings are the influence of the counter-ions on the biological properties of these complexes: (i) the complexes with a phosphonium ([P]) counter-ion in general favor the anticancer and antiplasmodial activity; (ii) the complexes with an ammonium ([N]) counter-ion favor the antibacterial/fungi activities; and (iii) the complexes with [P] counter-ion exhibited low toxicity in the zebrafish embryo model. Another feature is the nature of the exocyclic chalcogen atom, e.g., the exocyclic sulfur replacement by $= C(CN)_2$ increases the cytotoxic activity and the steric hindrance generated by the side chain, from Pr to *i*Pr, decreases the anticancer activity. Although this study uses a relatively modest set of compounds for a SARs approach revealing relationships between structural properties and biological activities, it represents the basis for the development of potent pharmaceutical agents.

In summary, our results show that these complexes are potentially valuable drug candidates and suitable for further pharmacological testing, in particular those that show very low toxicity in zebrafish embryos. Similar to cancer cells, parasites need to maintain cellular redox balance and rely on redox enzymes such as TrxR to control the levels of ROS in the cytosol and mitochondria. Considering the similarities between the basic biological aspects of cancer and parasites and the fact that some compounds developed for cancer treatment could also be able to target parasitic enzymes such as Auranofin, our gold complexes could be explored for the benefit of both conditions, placing these compounds on the cutting edge of new research approaches in medicinal chemistry.

Author Contributions: Y.L.G. performed the synthesis and the redox analysis of the gold bis(dithiolene) complexes. A.F.-F. prepared and analyzed the gold bis(diselenolene) complexes. O.J., T.R. and V.D. performed the X-ray data collections and the structure refinements. D.L. conceived, designed the complexes, coordinated the chemical section and wrote the article together with F.M. D.F. (Diana Fontinha), D.F. (Denise Francisco) and M.P. performed the antiplasmodial activity studies. M.M. performed the toxicity studies in zebrafish embryo. C.S., S.A.S. and J.H.L. performed the antibacterial and antifungal activity studies. I.B. and N.T. performed the anti-HIV activity studies. T.S.M. performed the studies of interaction with HAS. J.F.G. performed DNA electrophoresis. F.M. performed the mechanistic studies and coordinated the biological section. All authors have read and agreed to the published version of the manuscript.

References

1. Paprochcka, R.; Wiese-Szadkowska, M.; Janciauskiene, S.; Kosmalski, T.; Kulik, M.; Helmin-Basa, A. Latest developments in metal complexes as anticancer agents. *Coord. Chem. Rev.* **2022**, *452*, 214307.
2. Zhang, P.; Sadler, P.J. Redox-active metal complexes for anticancer therapy. *Eur. J. Inorg. Chem.* **2017**, *12*, 1541–1548.
3. Frei, A.; Zuegg, J.; Elliott, A.G.; Baker, M.; Braese, S.; Brown, C.; Chen, F.; Dowson, C.G.; Dujardin, G.; et al. Metal complexes as a promising source for new antibiotics. *Chem. Sci.* **2020**, *11*, 2627–2639.
4. Li, Z.-Y.; Shen, Q.-H.; Mao, Z.-W.; Tan, C.-P. Rising interest in the development of metal complexes in cancer immunotherapy. *Chem. Asian J.* **2022**, e202200270, https://doi.org/10.1002/asia.202200270.
5. Hossain, S.; Roy, P.K.; Ali, R.; Zakaria, C.; Zahan, K.-E. Selected pharmacological applications of 1st row transition metal complexes: A review. *Clin. Med. Res.* **2017**, *6*, 177–191.
6. Anthony, E.J.; Bolitho, E.M.; Bridgewater, H.E.; Carter, O.W.L.; Donnelly, J.M.; Imberti, C.; Lant, R.C.; Lermyte, F.; Needham, R.J.; Palau, M.; et al. Metallodrugs are unique: Opportunities and challenges of discovery and development. *Chem. Sci.* **2020**, *11*, 12888–12917.
7. Hartmann, J.T.; Lipp, H.-P. Toxicity of platinum compounds. *Expert Opin. Pharmacother.* **2003**, *4*, 889–901.
8. Hanif, M.; Hartinger, C.G. Anticancer metallodrugs: Where is the next cisplatin? *Future Med. Chem.* **2018**, *10*, 615–617.
9. Dasari, S.; Tchounwou, P.B. Cisplatin in cancer therapy: Molecular mechanisms of action. *Eur. J. Pharmacol.* **2014**, *740*, 364–378.
10. Ghosh, S. Cisplatin: The first metal based anticancer drug. *Bioorg. Chem.* **2019**, *88*, 102925.
11. Nardon, C.; Boscutti, G.; Fregona, D. Beyond platinums: Gold complexes as anticancer agents. *Anticancer Res.* **2014**, 34, 487–492.
12. Kim, J.H.; Reeder, R.; Parkin, S.; Awuah, S.G. Gold(I/III)-phosphine complexes as potent antiproliferative agents. *Sci. Rep.* **2019**, *9*, 12335.
13. Kou, L.; Wei, S.; Kou, P. Current progress and perspectives on using gold compounds for the modulation of tumor cell metabolism. *Front. Chem.* **2021**, *9*, 733463.
14. Bertrand, B.; Williams, M.R.M.; Bochmann, M. Gold(III) complexes for antitumor applications: An overview. *Chem. Eur. J.* **2018**, *24*, 11840.
15. Radisavljević, S.; Bratsos, I.; Scheurer, A.; Korzekwa, J.; Masnikosa, R.; Tot, A.; Masnikosa, R.; Gligorijević, N.; Radulović, S.; Simović, A.R. New gold pincer-type complexes: Synthesis, characterization, DNA binding studies and cytotoxicity. *Dalton Trans.* **2018**, *47*, 13696.
16. Bertrand, B.; Casini, A. A golden future in medicinal inorganic chemistry: The promise of anticancer gold organometallic compounds. *Dalton Trans.* **2014**, *3*, 4209–4219.
17. Fung, S.K.; Zou, T.; Cao, B.; Lee, P.-Y.; Fung, Y.M.E.; Hu, D.; Lok, C.-N.; Che, C.-M. Cyclometalated gold(III) complexes containing N-heterocyclic carbene ligands engage multiple anti-cancer molecular targets. *Angew. Chem. Int. Ed.* **2017**, *56*, 3892–3896.
18. Carboni, S.; Zucca, A.; Stoccoro, S.; Maiore, L.; Arca, M.; Ortu, F.; Artner, C.; Keppler, B.K.; Meier-Menches, S.M.; Casini, A.; et al. New variations on the theme of gold(III) C∧N∧N cyclometalated complexes as anticancer agents: Synthesis and biological characterization. *Inorg. Chem.* **2018**, *57*, 14852–14865.
19. Magherini, F.; Fiaschi, T.; Valocchia, E.; Becatti, M.; Pratesi, A.; Marzo, T.; Massai, L.; Gabbiani, C.; Landini, I.; Nobili, S.; et al. Antiproliferative effects of two gold(I)-N-heterocyclicarbene complexes in A2780 human ovarian cancer cells: A comparative proteomic study. *Oncotarget* **2018**, *9*, 28042–28068.
20. Liu, W.; Gust, R. Metal *N*-heterocyclic carbene complexes as potential antitumor metallodrugs. *Chem. Soc. Rev.* **2013**, *42*, 755–773.
21. Ssemaganda, A.; Low, L.M.; Verhoeft, K.R.; Wambuzi, M.; Kawoozo, B.; Nabasumba, S.B.; Mpendo, J.; Bagaya, B.S.; Kiwanuka, N.; Stanisic, D.I.; et al. Good, Gold(I) phosphine compounds as parasite attenuating agents for malaria vaccine and drug development. *Metallomics* **2018**, *10*, 444–454.
22. Dominelli, B.; Correia, J.D.G.; Kühn, F.E. Medicinal Applications of Gold(I/III)-Based Complexes Bearing *N*-Heterocyclic Carbene and Phosphine Ligands. *J. Organomet. Chem.* **2018**, *866*, 153–164.
23. Mora, M.; Gimeno, M.C.; Visbal, R. Recent advances in gold—NHC complexes with biological properties. *Chem. Soc. Rev.* **2019**, *48*, 447–462.

24. Liu, W.; Gust, R. Update on metal *N*-heterocyclic carbene complexes as potential anti-tumor metallodrugs. *Coord. Chem. Rev.* **2016**, *329*, 191–213.

25. Goetzfried, S.K.; Kapitza, P.; Gallati, C.M.; Nindl, A.; Cziferszky, M.; Hermann, M.; Wurst, K.; Kircher, B.; Gust, R. Investigations of the reactivity, stability and biological activity of halido (NHC)gold(I) complexes. *Dalton Trans.* **2022**, *51*, 1395–1406.

26. Yeo, C.I.; Ooi, K.K.; Tiekink, E.R.T. Gold-Based Medicine: A Paradigm Shift in Anti-Cancer Therapy? *Molecules* **2018**, *23*, 1410.

27. Zou, T.; Lok, C.-N.; Wan, P.-K.; Zhang, Z.-F.; Fung, S.-K.; Che, C.-M. Anticancer metal-N-heterocyclic carbene complexes of gold, platinum and palladium. *Curr. Opin. Chem. Biol.* **2018**, *43*, 30–36.

28. Rackham, O.; Nichols, S.J.; Leedman, P.J.; Berners-Price, S.J.; Filipovska, A. A gold(I) phosphine complex selectively induces apoptosis in breast cancer cells: Implications for anticancer therapeutics targeted to mitochondria. *Biochem. Pharmacol.* **2007**, *74*, 992–1002.

29. Porchia, M.; Pellei, M.; Marinelli, M. New insights in Au-NHCs complexes as anticancer agents. *Eur. J .Med. Chem.* **2018**, *146*, 709–746.

30. Goetzfried, S.K.; Gallati, C.M.; Cziferszky, M.; Talmazan, R.A.; Wurst, K.; Liedl, K.R.; Podewitz, M.; Gust, R. *N*-Heterocyclic carbene gold(I) complexes: Mechanism of the ligand scrambling reaction and their oxidation to gold(III) in aqueous solutions. *Inorg. Chem.* **2020**, *59*, 15312–15323.

31. Onodera, T.; Momose, I.; Kawada, M. Potential anticancer activity of auranofin. *Chem. Pharm. Bull.* **2019**, *67*, 186–191.

32. Radisavljević, S.; Petrović, B. Gold(III) complexes: An overview on their kinetics, interactions with DNA/BSA, cytotoxic activity, and computational calculations. *Front. Chem.* **2020**, *8*, 379.

33. Quintana, M.; Rodriguez-Rius, A.; Vellé, A.; Vives, S.; Miguel, P.J.S.; Triola, G. Dinuclear silver and gold bisNHC complexes as drug candidates for cancer therapy. *Bioorg. Med. Chem.* **2022**, *67*, 116814.

34. Meier-Menches, S.M.; Neuditschko, B.; Zappe, K.; Schaier, M.; Gerner, M.; Schmetterer, K.; Del Favero, G.; Bonsignore, R.; Cichna-Markl, M.; Koellensperger, G.; et al. An organometallic gold(I) bis-N-heterocyclic carbene complex with multimodal activity in ovarian cancer cells. *Chem. Eur. J.* **2020**, *26*, 15528–15537.

35. Ratia, C.; Soengas, R.G.; Soto, S.M. Gold-derived molecules as new antimicrobial agents. *Front. Microbiol.* **2022**, *13*, 846959.

36. Büssing, R.; Karge, B.; Lippmann, P.; Jones, P.G.; Brönstrup, M.; Ott, I. Gold(I) and gold(III) *N*-heterocyclic carbene complexes as antibacterial agents and inhibitors of bacterial thioredoxin reductase. *ChemMedChem* **2021**, *16*, 3402–3409.

37. Glišića, B.Đ.; Djuran, M.I. Gold complexes as antimicrobial agents: An overview of different biological activities in relation to the oxidation state of the gold ion and the ligand structure. *Dalton Trans.* **2014**, *43*, 5950–5969.

38. Fuchs, B.B.; RajaMuthiah, R.; Souza A.C.R.; Eatemadpour, S.; Rossoni,R.D.; Santos, D.A.; Junqueira, J.C.; Rice, L.B.; Mylonakis E. Inhibition of bacterial and fungal pathogens by orphaned drug auronofin. *Future Med Chem*. **2016**, *8*, 117–132.

39. Wiederhold, N.P.; Patterson, T.F.; Srinivasan, A.; Chaturvedi, A.K.; Fothergill, A.W.; Wormley, F.L.; Ramasubramanian, A.K.; Lopez-Ribot, J.L. Repurposing auranofin as an antifungal: In vitro activity against a variety of medically important fungi. *Virulence* **2017**, *8*, 138–142.

40. Frei, A. Metal Complexes, an Untapped Source of Antibiotic Potential? *Antibiotics* **2020**, *9*, 90.

41. Derbyshire, E.R.; Prudêncio, M.; Mota, M.M.; Clardy, J. Liver-stage malaria parasites vulnerable to diverse chemical scaffolds. *Proc. Natl. Acad. Sci. USA* **2012**, *109*, 8511–8516.

42. Molter, A.; Rust, J.; Lehmann, C.W.; Deepa, G.; Chiba, P.; Mohr, F. Synthesis, structures and anti-malaria activity of some gold(I) phosphine complexes containing seleno- and thiosemicarbazonato ligands. *Dalton Trans.* **2011**, *10*, 9810–9820.

43. Khanye, S.D.; Wan, B.; Franzblau, S.G.; Gut, J.; Rosenthal, P.J.; Smith, G.S.; Chibale, K. Synthesis and in vitro antimalarial and antitubercular activity of gold(III) complexes containing thiosemicarbazone ligands. *J. Organomet. Chem.* **2011**, *696*, 3392–3396.

44. Sannella, A.R.; Casini, A.; Gabbiani, C.; Messori, L. New uses for old drugs. Auranofin, a clinically established antiarthritic metallodrug, exhibits potent antimalarial effects in vitro: Mechanistic and pharmacological implications. *FEBS Lett.* **2008**, *582*, 844–847.

45. Hemmert, C.; Fabié, A.; Fabre, A.; Benoit-Vical, F.; Gornitzka, H. Synthesis, structures, and antimalarial activities of some silver(I), gold(I) and gold(III) complexes involving *N*-heterocyclic carbene ligands. *Eur. J. Med. Chem.* **2013**, *60*, 64–75.

46. Sousa, S.A.; Leitão, J.H.; Silva, R.A.L.; Belo, D.; Santos, I.C.; Guerreiro, J.F.; Martins, M.; Fontinha, D.; Prudêncio, M.; Almeida, M.; et al. On the path to gold: Monoanionic Au bisdithiolate complexes with antimicrobial and antitumor activities. *J. Inorg. Biochem.* **2020**, *202*, 110904.

47. Fontinha, D.; Sousa, S.A.; Morais, T.S.; Prudêncio, M.; Leitão, J.H.; Le Gal, Y.; Lorcy, D.; Silva, R.A.L.; Velho, M.F.G.; Belo, D.; et al. Gold(III) bis(dithiolene) complexes: From molecular conductors to prospective anticancer, antimicrobial and antiplasmodial agentes. *Metallomics* **2020**, *12*, 974–987.

48. Marcon, G.; Messori, L.; Orioli, P.; Cinellu, M.A.; Minghetti, G. Reactions of gold(III) complexes with serum albumin. *Eur. J. Biochem.* **2003**, *270*, 4655–4661.

49. Topală, T.; Bodoki, A.; Oprean, L.; Oprean, R. Bovine Serum Albumin Interactions with Metal Complexes. *Clujul Med.* **2014**, *87*, 215–219.

50. Eid, S.; Fourmigué, M.; Roisnel, T.; Lorcy, D. Influence of the thiazole backbone on the structural, redox, and optical properties of dithiolene and diselenolene complexes. *Inorg. Chem.* **2007**, *46*, 10647–10654.

51. Filatre-Furcate, A.; Barrière, F.; Roisnel, T.; Jeannin, O.; Lorcy, D. Conformational behavior, redox and spectroscopic properties of gold dithiolene complexes: [Au(iPr-thiazYdt)2]-1 (Y = O, S, Se]. *Inorg. Chim. Acta* **2018**, *469*, 255–263.

52. Busch, W.; Duis, K.; Fenske, M.; Maack, G.; Legler, J.; Padilla, S.; Strähle, U.; Witters, H.; Scholz, S. The zebrafish embryo model in toxicology and teratology. *Reprod. Toxicol.* **2011**, *31*, 585–588.

53. Chaves, R.S.; Guerreiro, C.S.; Cardoso, V.V.; Benoliel, M.J.; Santos, M.M. Toxicological assessment of seven unregulated drinking water disinfection by-products (DBPs) using the zebrafish embryo bioassay. *Sci. Total Environ.* **2020**, *742*, 140522.

54. Hanigan, D.; Truong, L.; Simonich, M.; Tanguay, R.; Westerhoff, P. Zebrafish embryo toxicity of 15 chlorinated, brominated, and iodinated disinfection by-products. *J. Environ. Sci.* **2017**, *58*, 302–310.

55. Ribeiro, S.; Torres, T.; Martins, R.; Santos, M.M. Toxicity screening of Diclofenac, Propranolol, Sertraline and Simvastatin using Danio rerio and Paracentrotus lividus embryo bioassays. *Ecotox. Environ. Saf.* **2015**, *114*, 67–74.

56. Gao, X.-P.; Feng, F.; Zhang, X.-Q.; Liu, X.-X.; Wang, Y.-B.; She, J.-X.; He, Z.-H.; He, M.-F. Toxicity Assessment of 7 Anticancer Compounds in Zebrafish. *Int. J. Toxicol.* **2014**, *33*, 98–105.

57. Chirullo, B.; Sgarbanti, R.; Limongi, D.; Shytaj, I.L.; Alvarez, D.; Das, B.; Boe, A.; DaFonseca, S.; Chomont, N.; Liotta, L.; et al. A candidate anti-HIV reservoir compound, auranofin, exerts a selective 'anti-memory' effect by exploiting the baseline oxidative status of lymphocytes. *Cell Death Dis.* **2013**, *4*, e944.

58. Rigobello, M.P.; Messori, L.; Marcon, G.; Cinellu, M.A.; Bragadin, M.; Folda, A.; Scutari, G.; Bindoli, A. Gold complexes inhibit mitochondrial thioredoxin reductase: Consequences on mitochondrial functions. *J. Inorg. Biochem.* **2004**, *98*, 1634–1641.

59. Pratesi, A.; Gabbiani, C.; Michelucci, E.; Ginanneschi, M.; Papini, A.M.; Rubbiani, R.; Ott, I.; Messori, L. Insights on the mechanism of thioredoxin reductase inhibition by gold *N*-heterocyclic carbene compounds using the synthetic linear selenocysteine containing C-terminal peptide hTrxR(488-499): An ESI-MS investigation. *J. Inorg. Biochem.* **2014**, *136*, 161–169.

60. Bian, M.; Fan, R.; Zhao, S.; Liu, W. Targeting the thioredoxin system as a strategy for cancer therapy. *J. Med. Chem.* **2019**, *62*, 7309–7321.

61. Becker, K.; Gromer, S.; Schirmer, R.H.; Müller, S. Thioredoxin reductase as a pathophysiological factor and drug target. *Eur. J. Biochem.* **2000**, *267*, 6118–6125.

62. Ashall, F. Cancer cells and parasites: Two of a kind. *Trends Biochem. Sci.* **1986**, *11*, 518–520.

63. Duesberg, P.; Madrioli, D.; McCormack, A.; Nicholson, J.M. Is carcinogenesis a form of speciation? *Cell Cycle* **2011**, *10*, 2100–2114.

64. Beckmann, S.; Grevelding, C.G. Imatinib makes a fatal impact on morphology, pairing stability, and survival of adult *Schistosoma mansoni* in vitro. *Int. J. Parasitol.* **2010**, *40*, 521–526.

65. Harbut, M.B.; Vilchèze, C.; Luo, X.; Hensler, M.E.; Guo, H.; Yang, B.; Chatterjee, A.K.; Nizet, V.; Jacobs, W.R.; Schultz, P.G.; et al. Auranofin exerts broad-spectrum bactericidal activities by targeting thiol-redox homeostasis. *Proc. Natl. Acad. Sci. USA* **2015**, *112*, 4453–4458.

66. Morais, T.S.; Santos, F.C.; Corte-Real, L.; Garcia, M.H. Exploring the effect of the ligand design on the interactions between [Ru(η5-C5H5)(PPh3)(N,O)][CF3SO3] complexes and human serum albumin. *J. Inorg. Biochem.* **2013**, *129*, 94–101.

67. García-Moreno, E.; Tomás, A.; Atrián-Blasco, E.; Gascon, S.; Romanos, E.; Rodriguez-Yoldi, M.J.; Cerrada, E.; Laguna, M. In vitro and in vivo evaluation of organometallic gold(I) derivatives as anticancer agents. *Dalton Trans.* **2016**, *45*, 2462–2475.

68. Gouvea, L.R.; Garcia, L.S.; Lachter, D.R.; Nunes, P.R.; de Castro Pereira, F.; Silveira-Lacerda, E.P.; Louro, S.R.W; Jorge, P.; Barbeira, S.; Teixeira, L.R. Atypical fluoroquinolone gold(III) chelates as potential anticancer agents: Relevance of DNA and protein interactions for their mechanism of action. *Eur. J. Med. Chem.* **2012**, *55*, 67–73.

69. Tunes, L.G.; Morato, R.E.; Garcia, A.; Schmitz, V.; Steindel, M.; Corrêa-Junior, J.D.; Dos Santos, H.F.; Frézard, F.; de Almeida, M.V.; Silva, H.; et al. Preclinical gold complexes as oral drug candidates to treat leishmaniasis are potent trypanothione reductase inhibitors. ACS Infect. Dis. **2020**, *6*, 1121–1139.

70. Lakowicz, J.R. *Principles of Fluorescence Spectroscopy*; Springer: Berlin/Heidelberg, Germany, 2006.

71. Ding, F.; Diao, J.; Yang, X.-L.; Sun, Y. Structural analysis and binding domain of albumin complexes with natural dietary supplement humic acid. *J. Lumin.* **2011**, *131*, 2244–2251.

72. Le Gal, Y.; Rajkumar, M.; Vacher, A.; Dorcet, V.; Roisnel, T.; Fourmigué, M.; Barrière, F.; Guizouarn, T.; Lorcy, D. A sulfur-rich π-electron acceptor derived from 5,5'-bithiazolidinylidene: Charge-transfer complex vs charge-transfer salt. *CrystEngComm* **2016**, *18*, 3925–3933.

73. Le Gal, Y.; Roisnel, T.; Auban-Senzier, P.; Bellec, M.; Íñiguez, J.; Canadell, E.; Lorcy, D. Stable metallic state of a neutral radical single-component conductor at ambient pressure. *J. Am. Chem. Soc.* **2018**, *140*, 6998−7004.

74. Tenn, N.; Bellec, N.; Jeannin, O.; Piekara-Sady, L.; Auban-Senzier, P.; Íñiguez, J.; Canadell, E.; Lorcy, D. A single-component molecular metal based on a thiazole dithiolate gold complex. *J. Am. Chem. Soc.* **2009**, *131*, 16961–16967.

75. Yzambart, G.; Bellec, N.; Nasser, G.; Jeannin, O.; Roisnel, T.; Fourmigué, M.; Auban-Senzier, P.; Íñiguez, J.; Canadell, R.; Lorcy, D. Anisotropic chemical pressure effects in single-component molecular metals based on radical dithiolene and diselenolene gold complexes. *J. Am. Chem. Soc.* **2012**, *134*, 17138−17148.

76. Filatre-Furcate, A.; Roisnel, T.; Fourmigué, M.; Jeannin, O.; Bellec, N.; Auban-Senzier, P.; Lorcy, D. Subtle steric differences impact the structural and conducting properties of radical gold bis(dithiolene) complexes. *Chem. Eur. J.* **2017**, *23*, 16004–16013.

77. Altomare, A.; Burla, M.C.; Camalli, M.; Cascarano, G.; Giacovazzo, C.; Guagliardi, A.; Moliterni, A.G.G.; Polidori, G.; Spagna, R. *SIR97*: A new tool for crystal structure determination and refinement. *J. Appl. Cryst.* **1999**, *32*, 115–119.

78. Sheldrick, G.M. A short history of SHELX. *Acta Cryst.* **2008**, *64*, 112–122.

79. Farrugia, L.J. WinGX and ORTEP for Windows: An update. *J. Appl. Cryst.* **2012**, *45*, 849–854.

80. Sheldrick, G.M. Crystal structure refinement with SHELXL. *Acta Cryst.* **2015**, *71*, 3–8.

81. Nakayama, G.R.; Caton, M.C.; Nova, M.P.; Parandoosh, Z. Assessment of the Alamar Blue assay for cellular growth and viability in vitro. *J. Immunol. Methods* **1997**, *204*, 205–208.

82. Ploemen, I.H.J.; Prudêncio, M.; Douradinha, B.G.; Ramesar, J.; Fonager, J.; van Gemert, G.-J.; Luty, A.J.F.; Hermsen, C.C.; Sauerwein, R.W.; Baptista, F.G.; et al. Visualisation and quantitative analysis of the rodent malaria liver stage by real time imaging. *PLoS ONE* **2009**, *4*, e7881.

83. Duthie, E.S.; Lorenz, L.L. *Staphylococcal coagulase*: Mode of action and antigenicity. *J. Gen. Microbiol.* **1952**, *6*, 95–107.

84. Minogue, T.D.; Daligault, H.A.; Davenport, K.W.; Bishop-Lilly, K.A.; Broomall, S.M.; Bruce, D.C.; Chain, P.S.; Chertkov, O.; Coyne, S.R.; Freitas, T.; et al. Complete genome assembly of *Escherichia coli* ATCC 25922, a serotype O6 reference strain. *Genome Announc.* **2014**, *2*, e00969-14.

85. Borst, A.; Raimer, M.T.; Warnock, D.W.; Morrison, C.J.; Arthington-Skaggs, B.A. Rapid acquisition of stable azole resistance by *Candida glabrata* isolates obtained before the clinical introduction of fluconazole. *Antimicrob. Agents Chemother.* **2005**, *49*, 783–787.

86. Gillum, A.M.; Tsay, E.Y.; Kirsch, D.R. Isolation of the *Candida albicans* gene for orotidine-5'-phosphate decarboxylase by complementation of *S. cerevisiae* ura3 and *E. coli* pyrF mutations. *Mol. Gen. Genet.* **1984**, *198*, 179–182.

87. Weinstein, M.P.; Patel, J.B.; Burnham, C.-A.; Campeau, S.; Conville, P.S.; Doern, C.; Eliopoulos, G.M.; Galas, M.F.; Humphries, R.M.; Jenkins, S.G.; et al. *Methods for Dilution Antimicrobial Susceptibility Tests for Bacteria That Grow Aerobically*, 11th ed.; CLSI Supplement M07; Wayne, P.A., Ed.; Clinical and Laboratory Standards Institute: Annapolis Junction, MD, USA, 2018.

88. Arendrup, M.C.; Cuenca-Estrella, M.; Lass-Flörl, C.; Hope, W. EUCAST technical note on the EUCAST definitive document EDef 7.2: Method for the determination of broth dilution minimum inhibitory concentrations of antifungal agents for yeasts EDef7.2 (EUCAST-AFST). *Clin. Microbiol. Infect.* **2012**, *18*, E246–E247.

89. Lambert, R.J.W.; Pearson, J. Susceptibility testing: Accurate and reproducible minimum inhibitory concentration (MIC) and non-inhibitory concentration (NIC) values. *J. Appl. Microbiol.* **2000**, *88*, 784–790.

90. Bártolo, I.; Santos, B.S.; Fontinha, D.; Machado, M.; Francisco, D.; Sepodes, B.; Rocha, J.; Mota-Filipe, H.; Pinto, R.; Figueira, M.E.; et al. Spiro-beta-lactam BSS-730A displays potent activity against HIV and Plasmodium. *ACS Infect. Dis.* **2021**, *7*, 421–434.

91. Reed, L.J.; Muench, H. A simple method of estimating fifty percent endpoints. *Am. J. Hyg.* **1938**, *27*, 493–497.

92. Holmgren, A.; Björnstedt, M. Thioredoxin and thioredoxin reductase. *Methods Enzymol.* **1995**, *252*, 199–208.

93. Beaven, G.H.; Chen, S.-H.; D'albis, A.; Gratzer, W.B. A spectroscopic study of the haemin—Human-serum-albumin system. *Eur. J. Biochem.* **1974**, *41*, 539–546.

94. Coutinho, A.; Prieto, M. Ribonuclease T1 and alcohol dehydrogenase fluorescence quenching by acrylamide: A laboratory experiment for undergraduate students. *J. Chem. Educ.* **1993**, *70*, 425–428.

95. Kubista, M.; Sjöback, R.; Eriksson, S.; Albinsson, B. Experimental correction for the inner-filter effect in fluorescence spectra. *Analyst* **1994**, *119*, 417–419.